Agricultural Water Management 282 (2023) 108279

Contents lists available at ScienceDirect

Agricultural Water Management

journal homepage: www.elsevier.com/locate/agwat

Assessing the effects of water resources allocation on the uncertainty propagation in the water–energy–food–society (WEFS) nexus

Yujie Zeng [a], Dedi Liu [a,b,*], Shenglian Guo [a], Lihua Xiong [a], Pan Liu [a], Jie Chen [a], Jiabo Yin [a,b], Zhenhui Wu [a], Wan Zhou [a]

[a] State Key Laboratory of Water Resources and Hydropower Engineering Science, Wuhan University, Wuhan 430072, China
[b] Hubei Province Key Lab of Water System Science for Sponge City Construction, Wuhan University, Wuhan 430072, China

ARTICLE INFO

Keywords:
Water–energy–food–society nexus
Uncertainty propagation
Water resources allocation
Copula function

ABSTRACT

The water–energy–food–society (WEFS) nexus is profiled for sustainable development. The WEFS nexus exhibits strong uncertainty owing to the stochasticity of model structure, and water availability uncertainty under climate change and human activities. The WEFS nexus remains highly risky, as the uncertainty propagation in the WEFS nexus under the regulation of water resources allocation has rarely been investigated. In this study, white Gaussian noises were integrated into a system dynamic model for the WEFS nexus simulation, transforming the nexus from deterministic to stochastic. Based on a Monte Carlo simulation of the stochastic WEFS nexus with water availability uncertainty, the copula function was applied to evaluate the joint distributions between water availability and water shortage rates in the upstream and downstream zones to investigate the uncertainty propagation in the WEFS nexus. The effects of water resources allocation on the uncertainty propagation were analyzed by setting different water resources allocation schemes. The proposed approach was applied to the mid–lower reaches of Hanjiang River basin in China as a case study. The results indicate that an effective water resources allocation scheme can ensure water supply, and diminish the impacts of water availability uncertainty on water supply through reservoir operation. The annual average water supply rate increased from 84.74% to 93.45%, and the standard deviation decreased from 3.37% to 1.78%. The high-level environmental awareness evoked by water or food shortages decreased significantly with smaller uncertainty. The co-evolution of the WEFS was ensured through its nexus. Water storage capacity was the vital factor to regulate the uncertainty propagation in the WEFS nexus. The impacts of upstream water availability uncertainty were efficiently regulated via reservoir operation for the zones with sufficient water storage capacity. Water supply was ensured and there was no significant response of the WEFS through its nexus to different water resources allocation schemes. If there was few water storage capacity in a zone, the water supply was remarkably influenced by the water availability uncertainty in the upstream zone. The water supply was difficult to ensure, and was sensitive to different water resources allocation schemes. The environmental awareness evoked by water or food shortages increased. The environmental awareness feedback under the impacts of the noises increased water demand uncertainty by altering the socioeconomic expansion, further increased WEFS uncertainty through its nexus, particularly when water availability was much smaller than water demand. The proposed approach can help quantify the effects of water resources allocation on the uncertainty propagation in the WEFS nexus and contribute to the sustainable development of the WEFS nexus.

1. Introduction

Water, energy, and food are the fundamental human resources (Bilgen, 2014; Vörösmarty et al., 2000; West et al., 2014). The interconnections across the water, energy, and food systems are increasingly tight and thus can be profiled as the water–energy–food (WEF) nexus to increase resource use benefits (Cai et al., 2018; D'Odorico et al., 2018; Hoff, 2011; Huntington et al., 2021; Zeng et al., 2019a). Human sensitivity has been integrated into the WEF nexus to take the physical and social processes in the nexus simultaneously, and the WEF nexus has been expanded into the water–energy–food–society (WEFS) nexus for the sustainable development (Di Baldassarre et al., 2019; Fuchs et al.,

* Corresponding author at: State Key Laboratory of Water Resources and Hydropower Engineering Science, Wuhan University, Wuhan 430072, China.
E-mail address: dediliu@whu.edu.cn (D. Liu).

https://doi.org/10.1016/j.agwat.2023.108279
Received 21 November 2022; Received in revised form 14 March 2023; Accepted 15 March 2023
Available online 28 March 2023

2017; Sivapalan et al., 2012; Zeng et al., 2022). The system dynamic model has been widely applied to mimic the co-evolution of the nexus owing to its flexibility in describing the dynamics within an integrated system (Feng et al., 2016; Simonovic, 2002). However, modeling the WEFS nexus exhibits significant uncertainties owing to deficiencies in the model structure, and the input uncertainties.

Deficiencies in the model structure mainly arises from a lack of knowledge in representing the real-life process of the WEFS nexus. Numerous studies have applied deterministic system dynamic model based on coupled ordinary differential equations to simulate the dynamics of the nexus (Feng et al., 2016; Li et al., 2019; Wu et al., 2022). The deterministic model revealed the interactions among variables of the WEFS nexus, and further helped to investigate the co-evolution of the nexus. Stochasticity underlies the key process of model structure of the WEFS nexus simulation (Guerra et al., 2021; Shoemaker et al., 2020; Vellend et al., 2014), and can lead to remarkable variability in the state variables of the nexus. However, the deterministic model is often incapable of identifying the stochasticity in its model structure of the WEFS nexus simulation, and ignores the risk of its results challenging the sustainable development goals. The stochasticity of the nexus was typically simulated by using noises method (Chen et al., 2021; Feng et al., 2019; Guttal and Jayaprakash, 2007). For example, An et al. (2021) employed the noises method to ordinary differential equations for the dynamics of the water supply, power generation, and environmental awareness (WPE), transforming the WPE nexus simulation from deterministic to stochastic. The probability density function (PDF) of the state variable was estimated from the stochastic WPE nexus simulation, which provided more information for risk management than a deterministic series from the deterministic WPE nexus simulation. Therefore, the noises method can effectively investigate the stochasticity of the WEFS nexus, and further contribute to the risk management of the WEFS nexus to achieve sustainable development goals.

Water availability is one of the primary inputs to the WEFS nexus simulation. Owing to the impacts of climate change and human activities, the water availability uncertainty is expanding (Her et al., 2019; Muller Schmied et al., 2014; Vetter et al., 2017), and an increase in the risk of water supply through the WEFS nexus is also evident (Govindan and Al-Ansari, 2019; Ji et al., 2020; Ma et al., 2020; Zeng et al., 2019b). The effects of water availability uncertainties on the nexus are described only as a whole basin, which cannot express the uncertainty propagation within the basin, especially from upstream to downstream via hydrologic connections (Moges et al., 2020; Silva et al., 2018; Zhang and Shao, 2018). Thus, the risks of water shortage may propagate from upstream to downstream. Adaptive measures to ensure water supply should thereby consider the water availability uncertainties not only from the local area, but also from the upstream areas. As the joint distributions of hydrologic variables have often been adopted to express the water availability uncertainty (Renard, 2011; Serinaldi, 2013), the copula function has been used as a hydrologic frequency analysis method to describe water availability uncertainty by binding multiple independent random variables into joint distributions (Chen et al., 2013; Karmakar and Simonovic, 2009; Nelsen, 2006). Therefore, the water availability uncertainty propagation from upstream to downstream can be assessed by the copula function.

The water supply assurance strategy often results from a water resources allocation model that takes the impacts of the water availability uncertainty through reservoir operation (Castelletti et al., 2010; Chen et al., 2016; He et al., 2022; Liu et al., 2010; Zeng et al., 2017). Numerous studies took the water availability uncertainty following the historical natural water flow, whereas the impacts of reservoir operation on the water availability uncertainty were overlooked or significantly simplified. The risks of the water supply, and even of WEFS might be overestimated, or underestimated. Water resources allocation simultaneously takes the reservoir operation and the hydrologic connections into account (Liu et al., 2018; Pedro-Monzonis et al., 2015; Zeng et al., 2021). Incorporating a water resources allocation model into WEFS simulation can improve the assessment of the uncertainty propagation in the WEFS nexus.

Our study aims to quantitatively assess the effects of water resources allocation on the uncertainty propagation in the WEFS nexus. The reminder of this paper is organized as follows: Section 2 introduces the framework for developing the stochastic WEFS nexus simulation with water availability uncertainty, and assessing the effects of water resources allocation on the uncertainty propagation in the WEFS nexus. Section 3 applies the framework to the mid–lower reaches of Hanjiang River basin in China. Section 4 presents the co-evolution results of the stochastic WEFS nexus simulation with water availability uncertainty, and discusses the effects of water resources allocation on the uncertainty propagation in the WEFS nexus. Section 5 concludes the study.

2. Method

The simulation of the interactions between water, energy, food and society systems is based on the deterministic dynamic model of the WEFS nexus proposed by Zeng et al. (2022). The WEFS nexus model is transformed from deterministic to stochastic through adding the white Gaussian noises to the ordinary differential equations to express the model structure uncertainty of the WEFS nexus simulation. To determine the impacts of the water availability uncertainty on the stochastic WEFS nexus simulation, the PDF of the water availability within basin is estimated by frequency analysis method. Discrete water availability samples are generated by the Monte Carlo method through its PDF. As water shortage is outputted from the stochastic WEFS nexus simulation with the inputs of the discrete water availability, discrete water shortage rates are defined by the ratios of water shortage to demand. The PDF of the water shortage rate is then determined by fitting the sample data. Thus, joint distributions of the water availability and water shortage rates can be obtained by copula function through connecting their marginal distributions. The joint distribution functions can quantify the uncertainty propagation in the WEFS nexus that are the uncertainties of water availability from upstream to downstream. As different water resources allocation schemes are inputted into the WEFS nexus simulation, the effects of water resources allocation on the uncertainty propagation in the WEFS nexus can be studied by the joint distribution functions. The framework is illustrated as Fig. 1.

2.1. Deterministic dynamic WEFS nexus model

To investigate the interactions between water, energy, food and society systems, Zeng et al. (2022) developed a deterministic system dynamic model, expanding the WEF nexus into the WEFS nexus. The Interactive River-Aquifer Simulation (IRAS) water resources allocation model (Loucks, 2002; Zeng et al., 2021) was integrated into the WEFS nexus model to quantify the impacts of water resources allocation on the co-evolution of the WEFS nexus.

The WEFS nexus comprises four modules: water system, energy system, food system, and society system modules. In the water system module, the water demand is firstly projected based on socioeconomic factors. The water demand and water availability are then inputted into the IRAS model to simulate water resources allocation, including the water release from reservoir based on Fig. 2 and Eqs. (1)–(7), and the water shortage experienced by water users by Eqs. (8)–(9). The water supply and agricultural water shortage rates outputted from the water system module are then inputted into energy and food system modules, respectively, to determine the energy and food shortages. The water, energy and food shortage rates are taken as the inputs of the society system module to determine the shortage awareness of water, energy and food, and further the environmental awareness. Once the environmental awareness exceeds its critical value, the environmental awareness feedback to constrain the socioeconomic factors in the water system module will be triggered to alleviate the stress on water, energy and food supplies. Further details can be retrieved from Zeng et al. (2022).

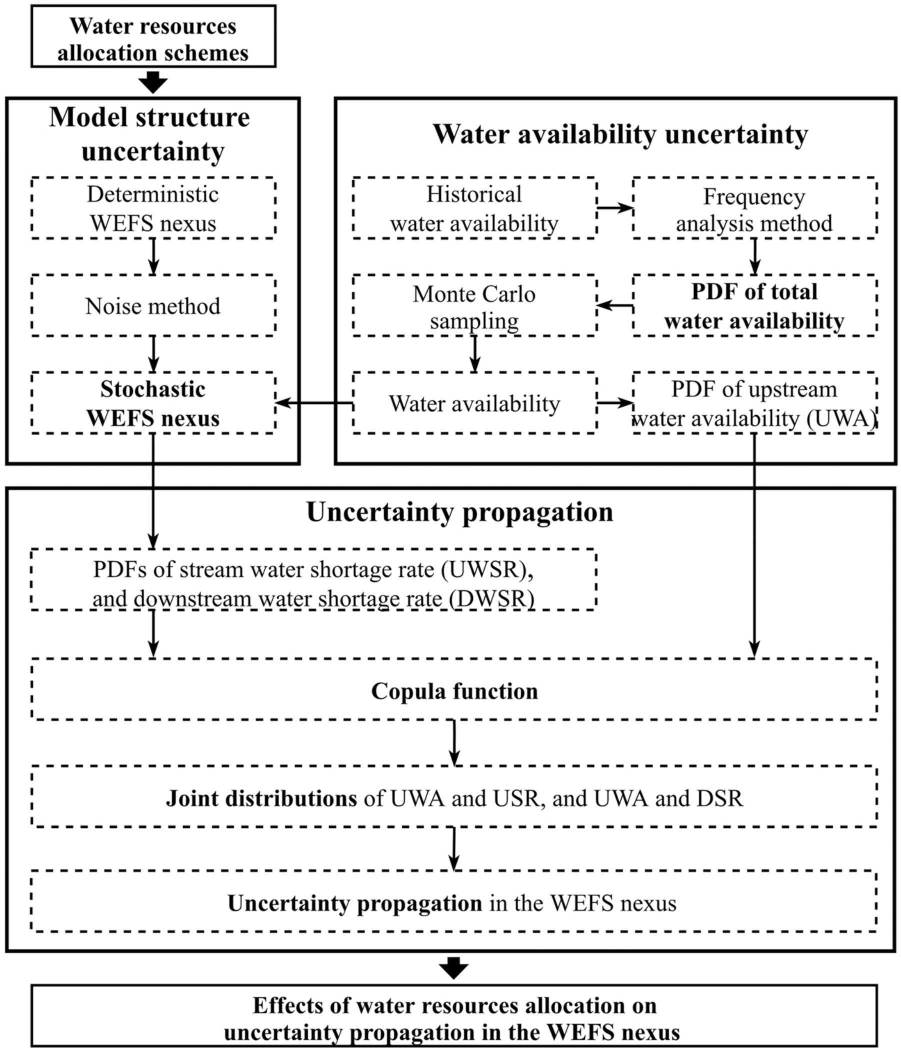

Fig. 1. Framework for assessing the effects of water resources allocation on the uncertainty propagation in the WEFS nexus.

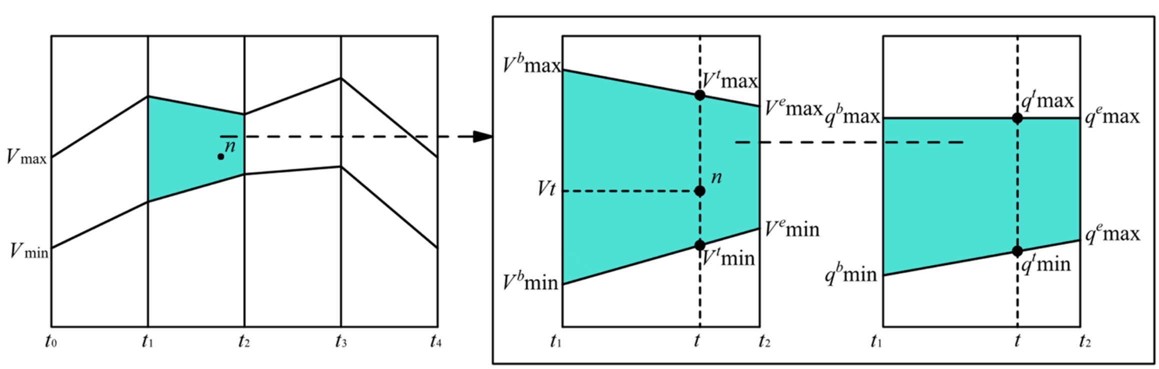

Fig. 2. Water release rule of reservoirs in the IRAS model.

$$P_t = (t - t_1)/(t_2 - t_1) \tag{1}$$

$$V^t_{max} = V^b_{max} * (1 - P_t) + V^e_{max} * P_t \tag{2}$$

$$V^t_{\min} = V^b_{\min} * (1 - P_t) + V^e_{\min} * P_t \tag{3}$$

$$q^t_{max} = q^b_{max} * (1 - P_t) + q^e_{max} * P_t \tag{4}$$

$$q^t_{min} = q^b_{min} * (1 - P_t) + q^e_{min} * P_t \tag{5}$$

$$P_v = (V^t - V^t_{\min})/(V^t_{\max} - V^t_{\min}) \tag{6}$$

$$q^t = q^t_{\min} * (1 - P_v) + q^t_{\max} * P_v \tag{7}$$

where t, t_1, and t_2 are the current time, initial time, and end time in the period, respectively; P_t denotes the ratio of current time length to period length; $V^t_{\max}$, $V^t_{\min}$, $V^b_{\max}$, $V^b_{\min}$, $V^e_{\max}$, and $V^e_{\min}$ represent the maximum and minimum storages at the current time, beginning, and ending of the period, respectively; $q^t_{\max}$, $q^t_{\min}$, $q^b_{\max}$, $q^b_{\min}$, $q^e_{\max}$, and $q^e_{\min}$ denote the maximum and minimum releases, respectively; P_v is the ratio of current storage; and q_t is the current release.

$$WE^{sts}_{i,j} = \left(\sum_{1}^{sts-1} WTSup^{sts}_{i,j} - \sum_{1}^{sts-1} WRSup^{sts}_{i,j}\right) * \frac{(Tsts - sts + 1)}{(sts - 1)} \tag{8}$$

$$WS^{sts}_{i,j} = \frac{WD^{ts}_{i,j}(1 - f_{red}) - \sum_{1}^{sts} WTSup^{sts}_{in} - WE^{sts}_{i,j}}{Tsts - sts + 1} \tag{9}$$

where ts is the current time step (in the IRAS model, the year is divided into user-defined time step, and each time step is broken into user-defined sub-time step, based on which water resources allocation conducts); $Tsts$ denotes the total number of the sub-time steps; sts is the current sub-time step; $WE^{sts}_{i,j}$ represents the projected natural water inflow for the j-th water use sector in the i-th operational zone; $WTSup^{sts}_{i,j}$ is the total water supply; $WRSup^{sts}_{i,j}$ is the water supply from reservoir; $WD^{ts}_{i,j}$ is the water demand; f_{red} is the demand reduction factor; and $WS^{st}_{i,j}$ is the water shortage.

2.2. Stochastic dynamic WEFS nexus model

As white Gaussian noise is popular in stochastic simulation owing to its effectiveness in capturing the randomness of state variables (Meng et al., 2020; Schmogrow et al., 2012; Xiao et al., 2021), it has been employed to simulate the stochasticity of the WEFS nexus. Specifically, the white Gaussian noises are incorporated into the seven primary governing equations (i.e., referring to the dynamics of population, GDP, crop area, water use quota, energy use quota, crop yield, and environmental awareness, respectively) to illustrate the uncertainties of the model structure of the WEFS nexus simulation as presented by Eqs. (10)–(16). The developed WEFS nexus simulation was transformed from deterministic into stochastic.

$$dN_t = r_{P,t} \cdot N_t \cdot dt + ts_P \cdot N_t \cdot dW_P \tag{10}$$

$$dG_t = r_{G,t} \cdot G_t \cdot dt + ts_G \cdot G_t \cdot dW_G \tag{11}$$

$$dCA_t = r_{CA,t} \cdot CA_t \cdot dt + ts_{CA} \cdot G_t \cdot dW_{CA} \tag{12}$$

$$dWQ^t_{i,j} = r_{qwu,t} \cdot WQ^t_{i,j} \cdot dt + ts_{qwu} \cdot WQ^t_{i,j} \cdot dW_{qwu} \tag{13}$$

$$dEQ^t_{i,j} = r_{e,t} \cdot EQ^t_{i,j} \cdot dt + ts_e \cdot EQ^t_{i,j} \cdot dW_e \tag{14}$$

$$dCY^t_{i,j} = r_{pro,t} \cdot CY^t_{i,j} \cdot dt + ts_{pro} \cdot CY^t_{i,j} \cdot dW_{pro} \tag{15}$$

$$dE_t = dWA_t + dEA_t + dFA_t + ts_{EN} \cdot E_t \cdot dW_{EN} \tag{16}$$

where N_t, G_t, CA_t, E_t, WA_t, EA_t, and FA_t, are the population, GDP, crop area, environmental awareness, shortage awareness of water, energy, and food in the t-th year, respectively; $WQ^t_{i,j}$, and $EQ^t_{i,j}$ denote the water, and energy use quotas of the j-th water user in the i-th operational zone, respectively; $CY^t_{i,j}$ is the potential crop yields of the j-th crop in the i-th operational zone; $r_{P,\ t}$, $r_{G,\ t}$, $r_{CA,\ t}$, $r_{qwu,\ t}$, $r_{e,\ t}$, and $r_{pro,\ t}$ are the growth rates of population, GDP, crop area, water use quota, energy use quota, and crop yield in the t-th year, respectively, which are the functions of time and environmental awareness feedback as detailed in Zeng et al. (2022); ts_P, ts_G, ts_{CA}, ts_{qwu}, ts_e, ts_{pro}, and ts_{EN} are the noise intensities for the growths of population, GDP, crop area, water use quota, energy use quota, crop yield, and environmental awareness, respectively; dW_P, dW_G, dW_{CA}, dW_{qwu}, dW_e, dW_{pro} and dW_{EN} are the white Gaussian noises for the growths of population, GDP, crop area, water use quota, energy use quota, crop yield, and environmental awareness, respectively.

2.3. Monte Carlo sampling for the water availability uncertainties

Monte Carlo sampling has been widely used to analyze the impacts of uncertain inputs or parameters of hydrological model on runoff (Jeremiah et al., 2011; Knighton et al., 2014). As runoff determines water availability, the water availability uncertainty can be analyzed by the Monte Carlo sampling. The PDF of a hydrologic variable, including water availability, is often described by the Pearson type III (P-III) distribution according to the recommendation in the specification for hydrologic computation of water resources and hydropower projects in China. The parameters of P-III distribution (shown as Eq. (17)) are estimated by minimizing the difference between the P-III distribution and the empirical distribution from the historical records of water availability.

$$f(x) = \frac{\beta^\alpha}{\Gamma(\alpha)}(x - a_0)^{\alpha-1}\exp(-\beta(x - a_0)), \alpha > 0, x > a_0 \tag{17}$$

where α, β, and a_0 are the shape, scale, and location parameters, respectively. The difference between empirical and the P-III distributions is quantified by the root-mean-square error (RMSE) as shown in Eq. (18).

$$RMSE = \sqrt{\frac{1}{n}\sum_{q=1}^{n} {e_q}^2} \tag{18}$$

where n is the sample size and e_q is the q-th differences of the sample. The maximum likelihood estimation is used to minimize the RMSE. Then, the Kolmogorov–Smimov (K–S) is adopted as a goodness-of-fit test for the optimal P-III distribution as a hypothesis testing. If the hypothesis testing with a 95% confidence interval is satisfied, the optimal distribution of water availability is acceptable for the Monte Carlo sampling of the stochastic WEFS nexus. The samples of the state variables can be obtained from the stochastic WEFS nexus simulation results.

To quantify the uncertainty of the state variables of the WEFS nexus, three indices that are the annual average value ($\bar{x}$), standard deviation (σ), and coefficient of variation (Cv) were adopted as shown in Eqs. (19), (20) and (21).

$$\bar{x} = \frac{1}{n}\sum_{q=1}^{n} x_q \tag{19}$$

$$\sigma = \sqrt{\frac{1}{n}\sum_{q=1}^{n}(x_q - \bar{x})^2} \tag{20}$$

$$Cv = \frac{\sigma}{\bar{x}} \tag{21}$$

where x_q is the q-th individual in the sample of the state variable and n is the sample size.

2.4. Uncertainty propagation in the WEFS nexus

The samples of the state variables of the WEFS nexus can be obtained from the stochastic WEFS nexus simulation inputted by the samples of water availability. As the stochastic WEFS nexus is nonlinear owing to the reservoir operation and heterogenetic input (e.g., water availability and water demand), the distributions of the output of the stochastic WEFS nexus (e.g., water shortage rate) might not be the same as that of the inputs (i.e., the P-III distribution). The normal, lognormal, exponential, gamma, Weibull, and generalized extreme value distributions were also tested to fit the distribution of water shortage rate. To investigate the uncertainty propagation in the WEFS nexus, the joint distributions of water availability and water shortage rates can be used to describe the uncertainty propagation. The copula function can link multiple independent variables into a multivariate distribution by effectively capturing system dependence, and has been extensively applied to multivariate uncertainty analysis of complex systems (Nelsen, 2006; Yin et al., 2018; Zhang et al., 2021b). It can be implemented to obtain the joint distributions after determining the distributions of water availability and water shortage rate as their marginal distributions according to the Sklar's theorem in Eq. (22).

$$F(x, y) = C(u, v) \tag{22}$$

where F is a joint distribution; C denotes a copula function; u and v denote the cumulative density functions of the variables x and y according to their marginal distribution functions, respectively. The Archimedean copula comprising the Gumbel-Hougaard, Clayton, and Frank copulas, Gaussian copula, and student copula (also named t copula) is easily constructed and can effectively capture extensive dependence structures with different desirable properties in hydrologic analysis. The copulas above are adopted here to construct the joint distributions of water availability and water shortage rate to describe the uncertainties propagation in the WEFS nexus.

Based on the joint distributions constructed by the copula function, it is easy to determine the cumulative density functions of water shortage rates in the upstream and downstream operational zones under varied water availability conditions of the upstream operational zones. The propagation of water availability uncertainty within the WEFS nexus or from upstream to downstream can be investigated through their conditional distribution functions. The effects of water resources allocation on the uncertainty propagation in the WEFS nexus are then assessed through inputting different water resources allocation schemes.

3. Case study

3.1. Study area

The Hanjiang River is the largest tributary of the Changjiang River. The mid–lower basin of Hanjiang River basin (MLHRB) covers 63,800 km^2 (shown in Fig. 3). The Danjiangkou reservoir, the water source of the middle route of the South–North water transfer project in China, is located at the upper boundary of MLHRB. The water availability in the MLHRB is thereby significantly affected by the reservoir operation of the water transfer project. The energy consumption in the MLHRB is considerable due to the large population and industry. As agriculture in the MLHRB is developed, the MLHRB is taken as one of the

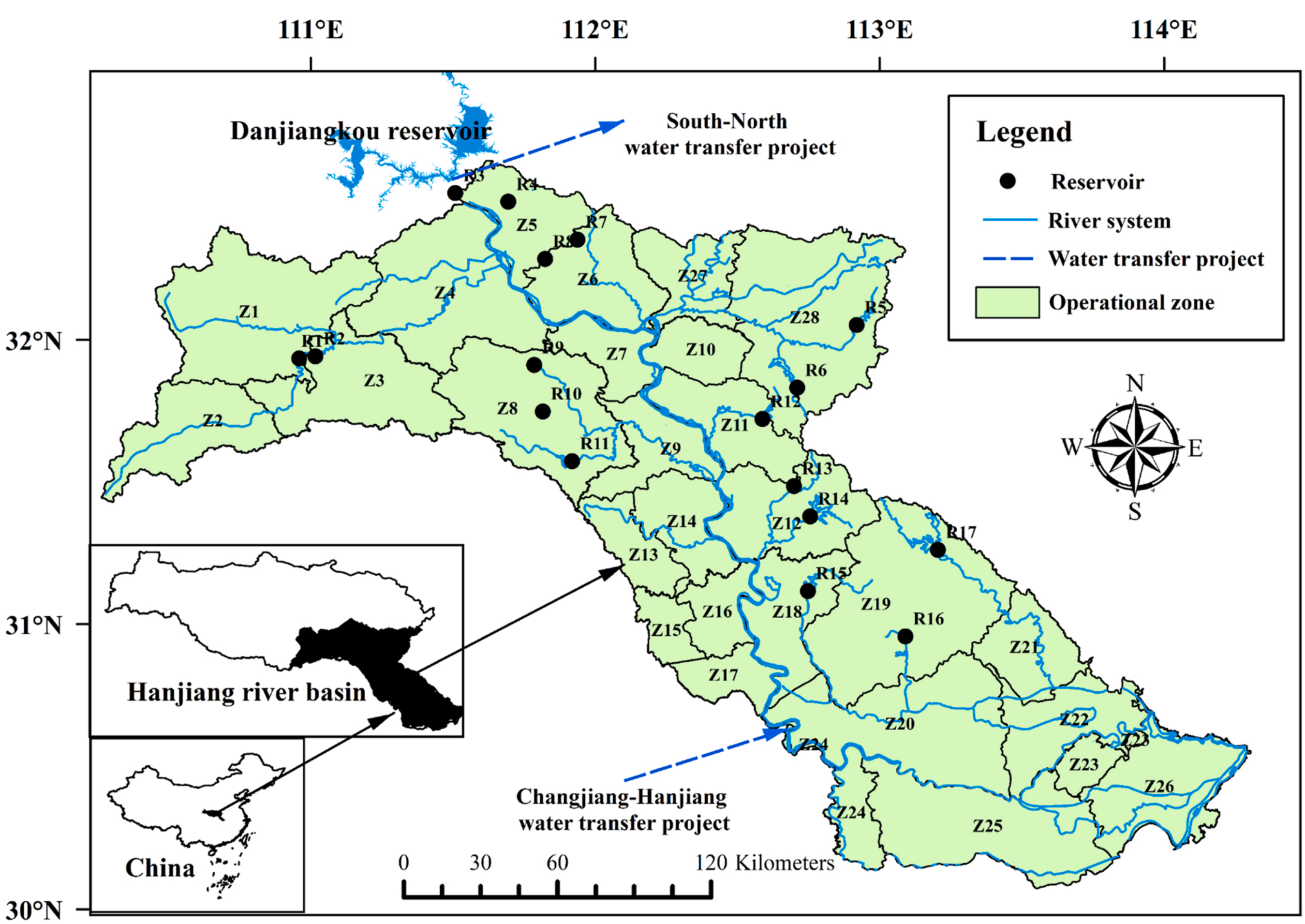

Fig. 3. The map of mid–lower reaches of the Hanjiang River basin.

nine major commodity grain bases in China. The interconnections across water, energy, food, and society systems in the MLHRB are intensifying due to socioeconomic development. With fast urbanization, the conflicts between the increasing the demands of water, energy and food and their supply capacities are aggravating, which has led to rising social concerns about resources shortages. The resources management strategy for water, energy and food based on the WEFS nexus is desirable to increase resource use efficiencies and benefits in production and consumption in the MLHRB. However, under the impacts of human activities and climate change, the water availability in the MLHRB exhibits strong uncertainty (Liu et al., 2018; Zeng et al., 2021). The water availability uncertainty can challenge the water, energy and food safeties in local area through the WEFS nexus, and may further propagate to downstream areas based on hydrologic connections. The downstream water, energy and food systems thus may be altered. Therefore, the MLHRB is taken as the study area to investigate the uncertainty propagation in the WEFS nexus.

Twenty-eight operational zones were sketched out by the superimposition of administrative units and sub-basins to maintain consistent socioeconomic and hydrological data in the operational zones. Five types of water users (i.e., municipal domesticity, rural domesticity, industry, agricultural, and in-stream ecology water users) were taken in each operational zone, resulting in 140 water users in the water resources allocation model. Seventeen medium and large size reservoirs (i.e., the total storage is more than 10 million m^3) and two water transfer projects were taken to regulate water availability in water resource allocation. The storage of all 17 reservoirs was 37.3 billion m^3. The operational zones, reservoirs, and water transfer projects within the water system in the MLHRB were sketched, as shown in Fig. 4.

3.2. Data sources

The WEFS nexus simulation was mainly driven by the hydrological and socioeconomic data. The monthly water availability data of each operational zone from 1956 to 2016 were obtained from the Changjiang Water Resources Commission (CWRC, 2016). The characteristics of the 17 reservoirs were retrieved from the Hubei Provincial Department of Water Resources (HPDWR, 2014) and were listed in Tables S1. The socioeconomic data from 2010 to 2019 were collected from the yearbooks of Hubei Province, including the annual population, GDP, crop area, water use quota, energy use quota, and crop yield, which were available at the Statistical Database of Chinese Economic and Social Development (http://data. cnki.net/). Notably, the agricultural water use quota is related to the precipitation frequency. Four typical exceedance frequencies (i.e., P = 50%, 75%, 90%, and 95% are related to the wet, normal, dry, extreme dry years, respectively), were estimated based on the frequency analysis method to predict the agricultural water demand series. These historical data were further inputted into the WEFS nexus model to predict the co-evolution of the WEFS nexus during 2010–2070 (Table 1).

Table 1
Forms of Gumbel-Hougaard, Clayton, Frank, Gaussian, and t copula functions.

Type	Copula expression	Range of θ
Gumbel-Hougaard	$\exp\{-[(-\ln u^{\theta})+(-\ln v^{\theta})]^{1/\theta}\}$	[1, ∞)
Clayton	$\max\,[(u^{-\theta}+v^{-\theta}-1)^{-1/\theta},0]$	(0, ∞)
Frank	$-\dfrac{1}{\theta}\ln\left[1+\dfrac{(e^{-\theta u}-1)(e^{-\theta v}-1)}{(e^{-\theta}-1)}\right]$	$R\backslash 0$
Gaussian	$\Phi_{\theta}[\Phi^{-1}(u),\Phi^{-1}(v)]$	[− 1, 1]
t	$t_{\theta,k}[t_k^{-1}(u),t_k^{-1}(v)]$	[− 1, 1]

where θ is a parameter to measure the degree of correlation between u and v; Φ is the standard normal distribution function; t is the student distribution function with k degree of freedom.

3.3. Scenarios with water resources allocation schemes

Combining the water availability and water resources allocation schemes, seven scenarios were set for the uncertainty analysis of the WEFS nexus as listed in Table 2. Scenario I was set as the reference one. Its water resources allocation scheme and the calibrated parameters for

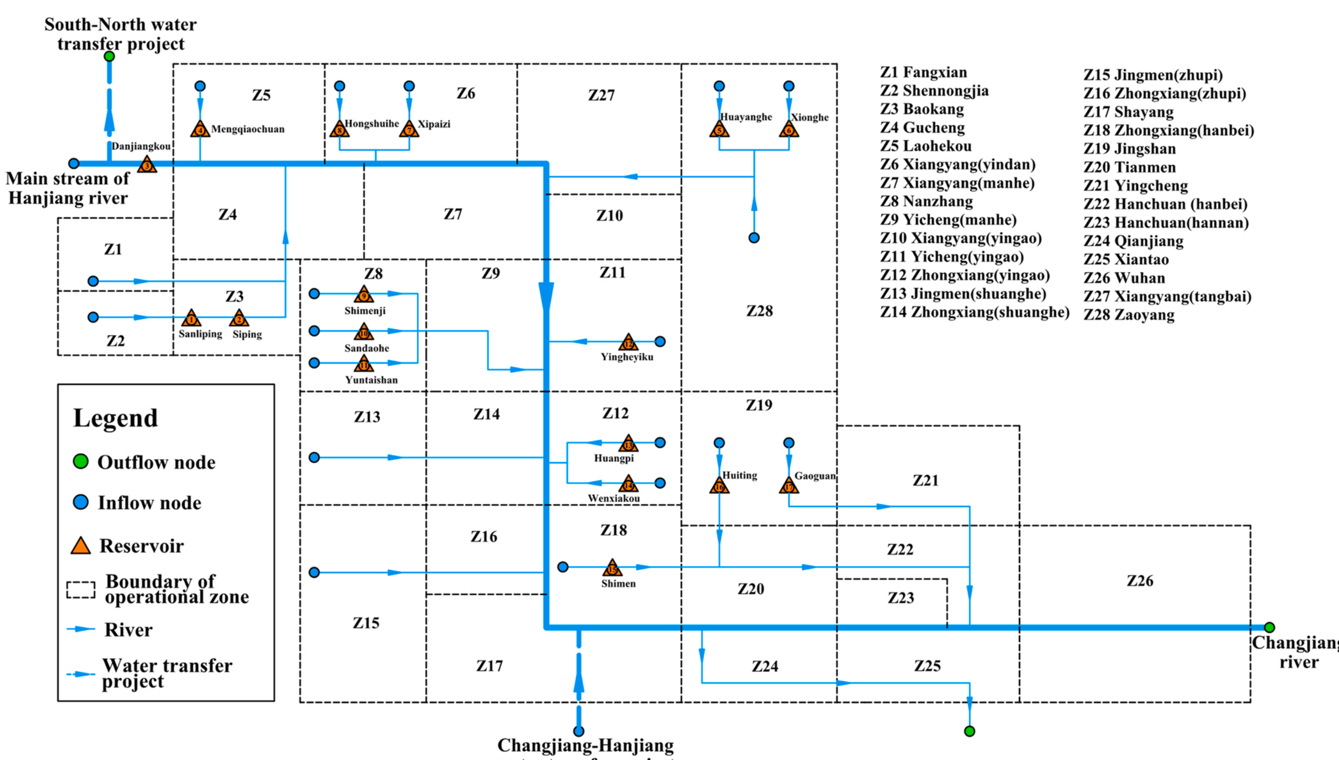

Fig. 4. The sketch graphic of mid–lower reaches of the Hanjiang River basin.

Table 2
Scenarios for the effects of water resources allocation on the uncertainty in the WEFS nexus [a].

Scenario	Water availability	Water resources allocation model	Parameter setting
I	WA_0	Yes	Calibrated values (Zeng et al., 2022)
II	WA_x	No	Critical values for water shortage rate is 0.15; others are calibrated values
III	WA_x	Yes	Calibrated values ($Q_{release}$ is 1.00)
IV	WA_x	Yes	$Q_{release}$ is 0.50; others are calibrated values
V	WA_x	Yes	$Q_{release}$ is 0.75; others are calibrated values
VI	WA_x	Yes	$Q_{release}$ is 1.25; others are calibrated values
VII	WA_x	Yes	$Q_{release}$ is 1.50; others are calibrated values

[a] WA_0 is the water availability from the historical hydrological data, while WA_x is the water availability sampled from its distribution for the uncertainty analysis.

the deterministic process of the WEFS nexus simulation were set by Zeng et al. (2022). The water availability was based on the historical record, while its WEFS nexus simulation was stochastic in scenario I. If there was no water resources allocation model and the water availability data were sampled from its distribution in the WEFS nexus simulation, the water availability uncertainty was analyzed for the WEFS nexus as scenario II after setting the critical values for water shortage rates from 0.07 to 0.15 to avoid the explosion of environmental awareness (Zeng et al., 2022). If there was the water resource allocation model in the WEFS nexus simulation, scenario III was set to analyze the impacts of water availability uncertainty on the WEFS nexus by comparing it with the scenarios II. The reservoir release multiplier ($Q_{release}$) was the ratio of the amount of water released from reservoir to that under the reference scenario according to reservoir operation rules. The $Q_{release}$ was used to indicate different water resources allocation schemes. Scenarios IV, V, VI, and VII were set to discuss the response of the WEFS nexus simulation to different water resources allocation schemes. According the sensitivity analysis results, the reservoirs release multiplier was set between 0.5 and 1.5 (Zeng et al., 2022). Scenarios IV, V, VI, and VII were set with their $Q_{release}$ at 0.5, 0.75, 1.25, and 1.5, respectively.

4. Results and discussion

The uncertainty of the WEFS nexus in the MLHRB was analyzed at monthly time step. The co-evolution of the WEFS nexus was from 2010 to 2070. Specifically, an initial parameter sensitivity analysis for the stochastic WEFS nexus was conducted to determine the noise intensities of the governing equations, as described in Section 2.2. The annual water availability from 1956 to 2016 was used to approximate the PDF of water availability. According to the monthly ratios of water availability based on the historical hydrological data, monthly water availability was obtained and inputted into the stochastic WEFS nexus simulation. The size of the Monte Carlo sampling was set to 1000 and the sample was tested to capture the PDFs of the state variables of the WEFS nexus, which were shown in Fig. S1. The outputs from the stochastic WEFS nexus simulation were used to analyze the uncertainty of the WEFS nexus. The joint and conditional distributions of water availability and water shortage rates at upstream and downstream operational zones were derived through copula function to analyze the uncertainty propagation in the WEFS nexus under the seven scenarios.

Table 3
Noise intensities for the stochastic WEFS nexus.

Variable	ts_P	ts_G	ts_{CA}	ts_{qwu}	ts_e	ts_{pro}	ts_{EN}
Noise intensity value	0.005	0.003	0.005	0.002	0.003	0.001	0.05

4.1. Uncertainty sources of the WEFS nexus in the MLHRB

The noise intensities are the key parameters for the stochastic process in the WEFS nexus simulation as presented in Eqs. (10)–(16). To ensure the co-evolution of the WEFS nexus within the rational intervals, an initial sensitivity analysis of the noise intensities was conducted to determine their values as listed in Table 3. The rational intervals of the socioeconomic state variables (i.e., population, GDP, crop area, water use quota, energy use quota, and crop yield) were based on their historical data, and all their noise intensities were no more than 0.005. There were no historical data for environmental awareness, as environmental awareness was a subjective variable that describes the societal perceptions of environmental degradation within the prevailing value systems. Environmental awareness was often reflected by media focus, and was thus accompanied with larger uncertainty than the variables with historical data. The noise intensity of environmental awareness was thus assumed to be 0.05 according to the initial sensitivity analysis.

The parameters of the P-III distribution for the total water availability in the entire MLHRB were estimated by the maximum likelihood estimation. Parameters α, β, and a_0 values were 9.60, 0.19 billion m^{-3} and 0.26 billion m^3, respectively. It was taken as the optimal distribution of the total water availability, with the RMSE of 0.0312. Thus, the PDF of the total water availability in the entire MLHRB was bell-shaped and positive-partial as shown in Fig. 5, and the total probability between 25 and 70 billion m^3 was more than 95%. The coefficients of variation (Cv) and skewness (Cs) were 0.645 and 0.321, respectively. The ratio of Cs to Cv was 2.01. The p-value was 0.8795 in the K–S test with a 95% confidence level, suggesting that the optimal P-III distribution was capable to describe the water availability uncertainty and laid the foundation for Monte Carlo sampling.

4.2. Effects of water resources allocation on the uncertainty of the WEFS nexus at the whole MLHRB

There are seven primary state variables in the WEFS nexus that are water demand, energy demand, food production, water supply rate, energy supply rate, food supply rate, and environmental awareness. These seven state variables were selected to investigate the potential

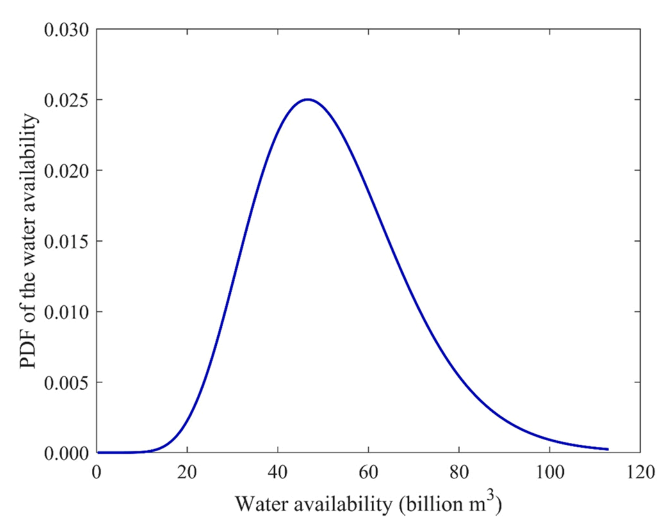

Fig. 5. The PDF of the optimal P-III distribution of the total water availability of the whole MLHRB.

Table 4
Water demand and water supply rate of every user resulted from water resources allocation model (Million m^3).

Scenario	Variable		Municipal domesticity	Rural domesticity	Industry	Agriculture	In-stream ecology	Total of all water users
I	Demand	$\overline{x}_{wd}$	387	181	6362	6314	3779	17,022
		σ_{wd}	11	5	108	176	0	233
	Supply	$\overline{x}_{ws}$	386	181	5728	5909	3695	15,901
		σ_{ws}	11	5	94	158	1	205
	Supply rate (%)	$\overline{x}_{wsr}$	99.78	99.81	90.11	93.65	97.79	93.45
		σ_{wsr}	0.01	0.01	0.06	0.12	0.02	0.08
II	Demand	$\overline{x}_{wd}$	297	143	1751	5876	3779	11,845
		σ_{wd}	45	19	498	611	0	715
	Supply	$\overline{x}_{ws}$	271	130	1333	4939	3290	9985
		σ_{ws}	42	18	422	589	90	761
	Supply rate (%)	$\overline{x}_{wsr}$	91.28	91.26	79.19	84.27	87.06	84.76
		σ_{wsr}	0.36	0.40	4.35	3.99	2.39	3.37
III	Demand	$\overline{x}_{wd}$	379	178	5456	6169	3779	15,961
		σ_{wd}	13	6	800	411	0	896
	Supply	$\overline{x}_{ws}$	378	177	4901	5752	3682	14,897
		σ_{ws}	13	6	734	418	41	888
	Supply rate (%)	$\overline{x}_{wsr}$	99.72	99.77	90.03	93.41	97.43	93.45
		σ_{wsr}	0.14	0.11	1.72	2.40	1.10	1.78
IV	Demand	$\overline{x}_{wd}$	370	174	4375	6149	3779	14,847
		σ_{wd}	16	7	982	449	0	1003
	Supply	$\overline{x}_{ws}$	369	173	3895	5696	3653	13,794
		σ_{ws}	16	7	888	460	54	977
	Supply rate (%)	$\overline{x}_{wsr}$	99.71	99.76	89.47	92.81	96.66	93.11
		σ_{wsr}	0.15	0.12	2.10	2.75	1.43	2.12
V	Demand	$\overline{x}_{wd}$	377	177	5024	6156	3779	15,513
		σ_{wd}	14	6	877	416	0	954
	Supply	$\overline{x}_{ws}$	376	176	4497	5715	3670	14,440
		σ_{ws}	14	6	798	426	46	936
	Supply rate (%)	$\overline{x}_{wsr}$	99.71	99.76	89.77	92.99	97.12	93.23
		σ_{wsr}	0.15	0.11	1.85	2.60	1.22	1.93
VI	Demand	$\overline{x}_{wd}$	381	178	5488	6185	3779	16,010
		σ_{wd}	14	6	838	444	0	949
	Supply	$\overline{x}_{ws}$	380	178	4937	5777	3688	14,965
		σ_{ws}	13	6	772	449	40	941
	Supply rate (%)	$\overline{x}_{wsr}$	99.72	99.78	90.18	93.57	97.59	93.60
		σ_{wsr}	0.14	0.11	1.75	2.45	1.07	1.80
VII	Demand	$\overline{x}_{wd}$	379	178	5380	6181	3779	15,896
		σ_{wd}	14	6	878	447	0	986
	Supply	$\overline{x}_{ws}$	378	177	4840	5769	3688	14,859
		σ_{ws}	14	6	808	453	41	976
	Supply rate (%)	$\overline{x}_{wsr}$	99.72	99.78	90.19	93.51	97.60	93.61
		σ_{wsr}	0.15	0.12	1.82	2.55	1.10	1.87

Table 5
Energy demand, food production, energy supply rate, food supply rate, and environmental awareness resulted from the WEFS nexus simulation.

Variable Scenario		I	II	III	IV	V	VI	VII
Energy demand (Million kw*h)	$\overline{x}_{ec}$	1745	515	1521	1248	1412	1531	1504
	σ_{ec}	27	127	199	243	217	209	219
Food production (Thousand ton)	$\overline{x}_{fp}$	6529	5572	6362	6309	6327	6391	6389
	σ_{fp}	178	624	456	500	463	487	497
Energy supply rate (%)	$\overline{x}_{esr}$	92.57	100.00	96.75	98.88	97.84	96.51	96.81
	σ_{esr}	1.25	0.00	2.29	1.38	1.86	2.64	2.58
Food supply rate (%)	$\overline{x}_{fsr}$	98.88	90.39	97.90	97.38	97.61	97.96	97.88
	σ_{fsr}	0.31	7.21	1.93	2.35	2.14	1.91	2.02
Environmental awareness	$\overline{x}_{E}$	5.83	14.75	7.46	9.29	8.34	7.23	7.36
	σ_{E}	0.63	5.05	2.03	2.55	2.21	2.14	2.21

effects of the water resources allocation on the total uncertainty of the WEFS nexus. The water supply priorities in the IRAS model from high to low were assigned as municipal and rural domesticity, in-stream ecology, industrial and agricultural users according to the Integrated Water Resources Planning of Hanjiang River Basin (CWRC, 2016). Table 4 listed water demand and water supply resulting from the water resources allocation model under seven scenarios. Table 5 listed the remaining five state variable values (i.e., energy demand, food production, energy supply rate, food supply rate, and environmental awareness) that were outputted from the WEFS nexus simulation. The average $\overline{x}$ and standard deviation σ from the samples quantified their uncertainties throughout the co-evolution process. To illustrate the evolution processes of the state variables of the stochastic WEFS nexus under the impacts of water availability uncertainty and water resources allocation, the trajectories of the average values and the intervals at 95% confidence level under scenarios I, II, and III were determined and shown in Fig. 6.

4.2.1. *Response of the uncertainty of the WEFS nexus to water resources allocation*

To investigate the stochasticity of the WEFS nexus, the results of scenario I showed that the co-evolution of the WEFS nexus simulation

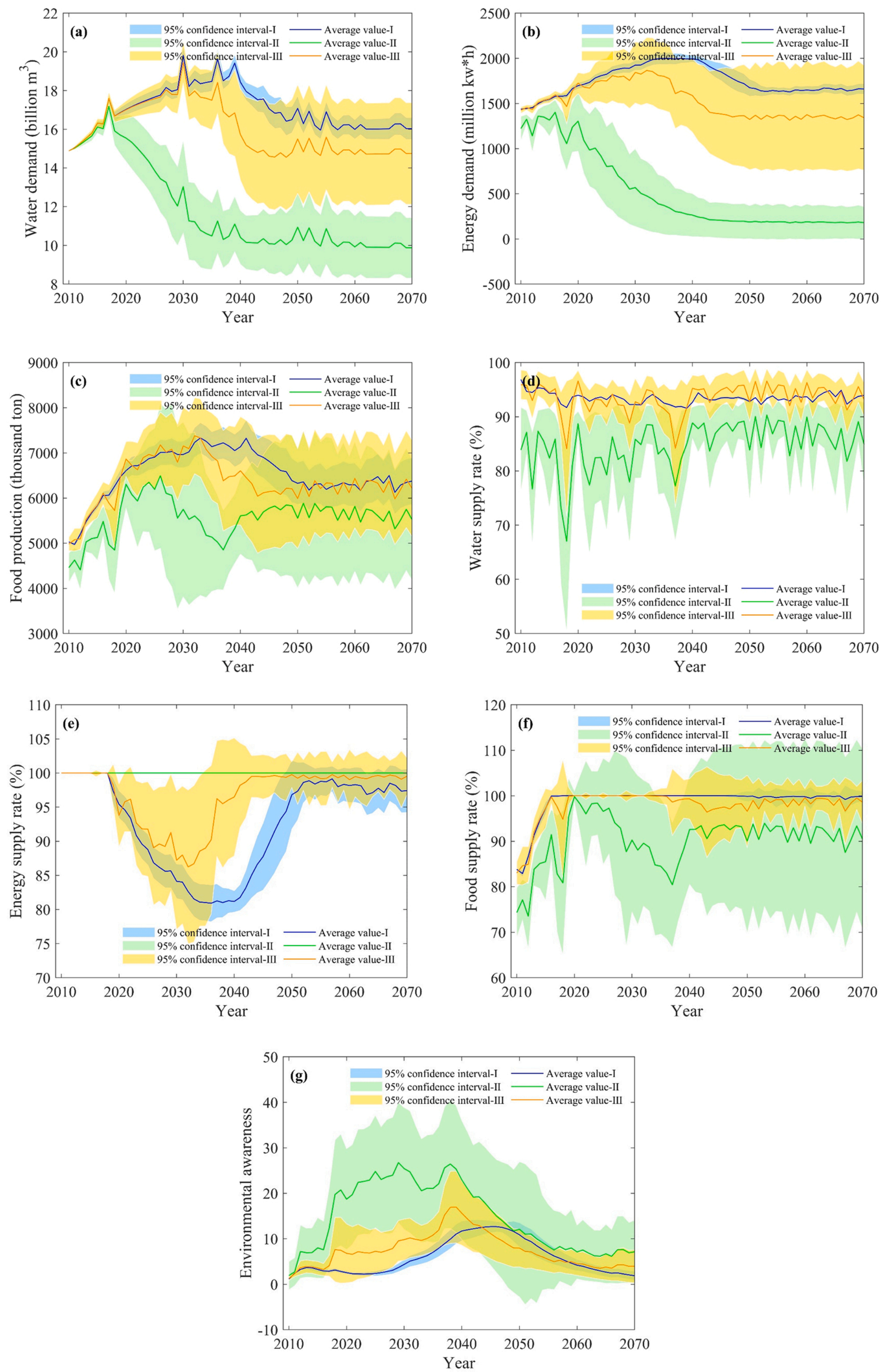

Fig. 6. Intervals of the seven state variables under scenarios I, II, and III at 95% confidence level: (a) water demand, (b) energy demand, (c) food production, (d) water supply rate, (e) energy supply rate, (f) food supply rate, and (g) environmental awareness.

was slightly altered by the noises. Water demand was directly affected by socioeconomic variables (i.e., population, GDP, crop area, and their water use quotas) as shown in Fig. 6(a). The average water demand was 17.02 billion m^3 and its standard deviation was 0.23 billion m^3. The water demand was satisfied and the water supply rate (shown in Fig. 6 (d)) showed little response to the noises. The uncertainty of the agricultural water supply was small, with a standard deviation of 0.12%, which accounted for that the food production increased with small uncertainty shown in Fig. 6(c). The average food production was 6529 thousand tons, with a standard deviation of 178 thousand tons. For the energy system, the energy demand in the water supply process with a small standard deviation of 27 million kw*h was altered by the water supply shown in Fig. 6(b). However, the total planning energy availability was less than the energy demand owing to socioeconomic expansion. The energy supply cannot be ensured. And the energy supply rate was typically lower than its critical value (i.e., 95% as detailed in Zeng et al., 2022), as shown in Fig. 6(e), which led to the accumulation of environmental awareness. The variability in the energy supply rate contributed to the uncertainty in the evolution of environmental awareness as shown in Fig. 6(g). As the environmental awareness often kept at a low level, and rarely exceeded its critical value of 8.0 in the evolution process shown in Fig. 6(g), the environmental awareness feedback on socioeconomic variables was rarely triggered, or only triggered with little intensity. Thus, the impacts of the uncertainty of environmental awareness owing to its noises on the WEFS nexus were not evident.

The impacts of water availability uncertainty on the stochastic WEFS nexus were determined by comparing the differences in the results between scenarios I and III. The WEFS nexus was remarkably altered by the water availability uncertainty. The average water demand decreased from 17.02 billion m^3 under scenario I to 15.96 billion m^3 under scenario III, while its standard deviation increased from 0.23 to 0.90 billion m^3. Although there were few differences in the supply rates of water, energy, and food between scenarios I and III, their standard deviations increased remarkably. The average environmental awareness increased from 5.83 under scenario I to 7.46 under scenario III, and its standard deviation simultaneously increased from 0.63 to 2.63. The increasing uncertainty of environmental awareness further led to larger variability of the co-evolution of the WEFS nexus through environmental awareness feedback under the impacts of noises.

The differences between the scenarios II and III can indicate the impacts of water resources allocation on the uncertainty of the WEFS nexus. The purpose of the water resources allocation model was to ensure water supply. The total water supply rate increased from 84.74% to 93.45%, and the standard deviation decreased from 3.37% to 1.78% under the scenarios II and III, respectively. As the water resources allocation model was integrated with scenarios III, the water supply rates of industrial and agricultural users increased from 79.19% and 84.27% to 90.03% and 93.4%, respectively. Their standard deviations also decreased from 4.35% and 3.99% to 1.72% and 2.40%, respectively. Thus, the uncertainties decreased. As much water was stored in the reservoirs during the flood season, and released during the dry season, the water shortage was remarkably alleviated due to the uneven temporal distribution of water availability. The impacts of the variability of the monthly water availability were also decreased, as the water inflow was stored in reservoirs based on seasonal or annual operational rules. The impacts of the uncertainties of water availability on water supply were thereby alleviated through reservoir operation under the scenarios III. With the increased agricultural water supply rate, the food production increased from 5572 to 6362 thousand tons. The considerable average environmental awareness caused by the water shortage and food shortage thereby decreased from 14.75 to 7.46, with smaller uncertainty. Negative feedback driven by environmental awareness then resulted in lower uncertainty for the co-evolution of the WEFS nexus.

There are four phases in the co-evolution of the WEFS nexus when water resources allocation was considered: expansion, contraction, recession, and recovery phases (Zeng et al., 2022). As the WEFS nexus performed differently in different phases, the response of WEFS nexus uncertainty to water resources allocation was analyzed in these four phases for the entire MLHRB under scenario III. In the expansion phase (i.e., 2010–2032), most water and energy demands can be satisfied. The accumulation of environmental awareness was mainly due to food shortages, as shown in Fig. 6(f). As water resources allocation can effectively alleviate the impacts of water availability uncertainty on water supply, the uncertainties in agricultural water supply and food production decreased. Although environmental awareness increased with increasing water and food shortages, the 95% confidence interval of environmental awareness was small as shown in Fig. 6(g). The socioeconomic sectors and the WEFS nexus can expand with a high confidence level in the expansion phase. However, during the contraction (i.e., 2033–2039) and recession phases (i.e., 2040–2045), as water availability could not cover the increasing water demand, most water was directly released from the reservoir rather than being stored in reservoir. Water availability was poorly regulated by reservoir. Thus, the water availability uncertainty directly impacted the water supply and increased the uncertainties of the evolution of energy demand and the food production through the WEFS nexus shown in Fig. 6(b) and (c). As the environmental awareness was positively correlated with water and energy shortage rates, environmental awareness exhibits high uncertainty due to the high uncertainties of water and energy shortage rates in the contraction and recession phases. The evolution of socioeconomic variables was altered by environmental awareness feedback under the impacts of noises. The water demand projected by the socioeconomic variables thereby also exhibited uncertainty. Although environmental awareness decreased in the recovery phase (i.e., 2046–2070), its uncertainty was not negligible in the co-evolution of the WEFS nexus through the dynamics of the state variables at the end of the recession phase. Therefore, water resources allocation can effectively decrease the water supply uncertainty through reservoirs operation. The uncertainty in the WEFS nexus also decreases. However, if the water demand exceeds the regulating capacity of the water system, the reservoirs can poorly regulate the water flow, and the stress on water supply increases. Water availability uncertainty can remarkably impact the water supply, and leads to the high uncertainties in the WEFS through its nexus.

4.2.2. Impacts of water resources allocation schemes on the uncertainty of the WEFS nexus

To obtain the optimal water resources allocation scheme, it was necessary to conduct the different water resources allocation schemes for the uncertainty of the WEFS nexus. The differences among scenarios III, IV, V, VI, and VII indicated the sensitivities of the uncertainty of the WEFS nexus to the reservoir release multipliers ($Q_{release}$). There were few differences in the water supply rate, ranging from 93.11% to 93.61% among these five scenarios. Water availability was abundant across the entire MLHRB, so the water demand was often satisfied. The standard deviations of water supply rate were 2.12%, 1.93%, 1.78%, 1.80%, and 1.87% under the scenarios IV, V, III, VI, and VII, respectively, and they were not linear with the $Q_{release}$ values. As less water was released with a smaller $Q_{release}$ value (e.g., the $Q_{release}$ of scenarios IV, and V were 0.50, and 0.75, respectively), more water was stored in the reservoir. Once the water level exceeded the normal water level of the reservoir, water was directly released downstream through the spillway. More water released from reservoir with larger $Q_{release}$ values (e.g., the $Q_{release}$ under scenarios VI, and VII were 1.25, and 1.50, respectively), and the regulation on water availability through the reservoir decreased. The water availability uncertainty slightly decreased. Thus, the uncertainty in the corresponding water supply cannot be efficiently alleviated by reservoir operation. The standard deviations of energy demand and food production further increased from 199 million kw*h and 456 thousand tons under scenario III to 209, 219 million kw*h, and 487, 497 thousand tons under scenarios VI and VII, respectively. These uncertainties in water supply, energy demand and food production have influenced socioeconomic expansion through environmental awareness feedback. The uncertainty in the corresponding socioeconomic water demand has increased. Therefore, policymakers should pay more attention to the regulating capacity of reservoirs in water resources management in a basin, which is an effective way to decrease the impacts of water availability uncertainties on water demand to ensure the co-evolution of the WEFS nexus.

4.3. *Effects of water resources allocation on the uncertainty propagation in the WEFS nexus within the MLHBR*

Water resources allocation can effectively alleviate the impacts of the water availability uncertainty on the water supply through reservoir operation to ensure the co-evolution of the WEFS nexus. However, as the water flows from upstream to downstream, water availability uncertainty also propagates from upstream to downstream. The responses of water supply, energy demand and food production to the uncertainty of water availability differed in upstream and downstream areas owing to the uneven distribution of reservoirs within the basin. According to the responses of the water supply from the water resources allocation model to the water availability uncertainty in every operational zone, the operational zones in the MLHRB can be categorized into three types shown in Fig. 7. If the water supply could be assured and impacted by the water availability uncertainty in an operational zone, the zone was taken as type A. If the water shortage can be effectively alleviated by water resources allocation, and the impacts of water availability uncertainty on water supply can be remarkably alleviated, the zone was taken as type B. There was no negligible water shortage in a zone, and its water supply was remarkably affected by the water availability uncertainty, the zone was taken as type C. Considering the hydrologic connections between the upstream and downstream zones, four types of routes for uncertainty propagation within the MLHRB can be found. The route (i) was from type A to type A zones, whereas the route (ii) was from type B to a type A zones. The route (iii) was from type B to type B zones, whereas the route (iv) was from type C to type A zones. Specifically, eight operational zones selected to show the uncertainty propagation in the WEFS nexus within the MLHRB: Z25 (Xiantao) and Z26 (Wuhan) with the route (i), Z2 (Shennongjia) and Z3 (Baokang) with the route (ii), Z19 (Jingshan) and Z21 (Yingcheng) with the route (iii), and Z13 (Jingmenshuanghe) and Z14 (Zhongxiangshuanghe) with the route (iv). The average and standard deviation values of the water demand, water supply rate, energy demand, and food production were listed in Table 6. As water availability for an operational zone contains water flows from upstream in addition to the local water availability, Table 7 listed the water availability from an upstream zone. Thus, water availability uncertainty can propagate from upstream to downstream. The uncertainty of the WEFS nexus varied in different phases during the co-evolution of the WEFS nexus as discussed in Section 4.2.1. The uncertainty emerged in the contraction phase, which was the vital phase. Therefore, a representative year 2035 in the contractions phase was selected to study the uncertainty propagation. The water flowing from the upstream to downstream operational zones were listed in Table 7.

4.3.1. *Response of the uncertainty propagation in the WEFS nexus to water resources allocation*

The response of uncertainty propagation in the WEFS nexus to water resources allocation varied through different routes. The uncertainty of upstream water availability was remarkably alleviated when it propagated downstream through the routes (i), (ii), and (iv), whereas it was not efficiently alleviated through the route (iii) in the case study. Taking the uncertainty propagation routes (iv) as an example, the water supply rate in Z13 was slightly increased by water resources allocation, from 62.32% under scenario II to 65.40% under scenario III, as there was few

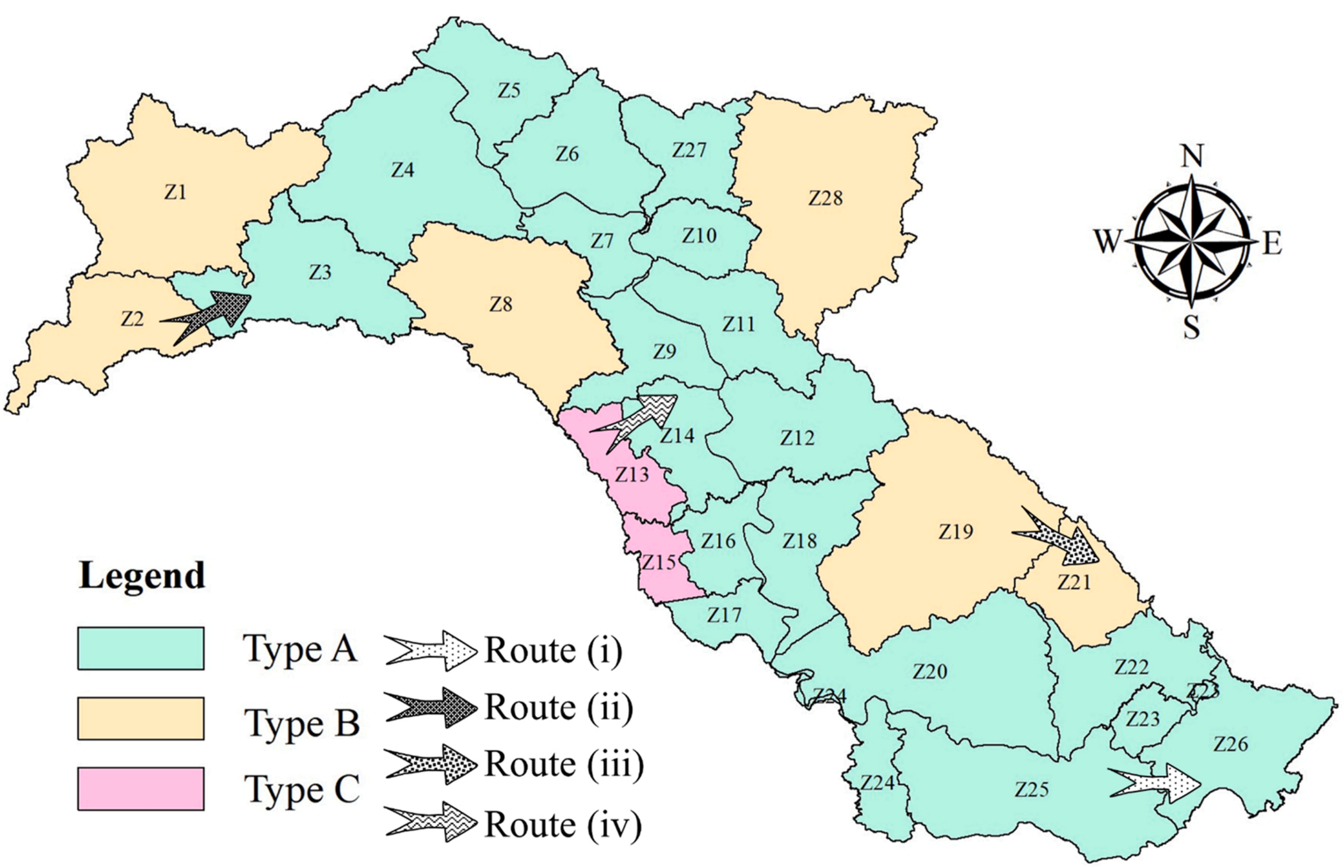

Fig. 7. Spatial distributions of operational zones of type A, B, and C.

Table 6
Water demand, water supply rate, energy demand, and food production in the eight operational zones.

Scenario	Variable		Z2	Z3	Z13	Z14	Z19	Z21	Z25	Z26
I	Water demand	$\bar{x}_{wd}$	315	204	192	249	520	369	1237	1607
	(Million m^3)	σ_{wd}	4	1	4	2	7	7	15	24
	Water supply	$\bar{x}_{ws}$	78.08	100.00	65.43	100.00	89.83	98.55	99.98	99.94
	rate (%)	σ_{ws}	0.45	0.00	0.72	0.00	0.49	0.23	0.01	0.01
	Energy demand	$\bar{x}_{ec}$	8	4	4	22	94	27	214	230
	(Million kw*h)	σ_{ec}	0	0	0	0	1	0	4	4
	Food production	$\bar{x}_{fp}$	6	29	35	81	365	274	712	327
	(Thousand ton)	σ_{fp}	0	1	1	2	10	7	20	9
II	Water demand	$\bar{x}_{wd}$	275	196	170	193	248	307	685	975
	(Million m^3)	σ_{wd}	13	2	12	8	31	21	62	79
	Water supply	$\bar{x}_{ws}$	67.80	90.21	62.32	91.62	84.42	86.06	91.03	89.64
	rate (%)	σ_{ws}	8.19	1.94	9.20	0.64	4.63	4.48	1.24	2.93
	Energy demand	$\bar{x}_{ec}$	2	2	1	7	26	12	61	62
	(Million kw*h)	σ_{ec}	1	0	0	2	7	2	16	17
	Food production	$\bar{x}_{fp}$	6	24	32	69	332	224	606	273
	(Thousand ton)	σ_{fp}	1	3	5	7	42	27	66	31
III	Water demand	$\bar{x}_{wd}$	306	202	187	238	466	356	1128	1479
	(Million m^3)	σ_{wd}	10	2	8	10	46	16	94	108
	Water supply	$\bar{x}_{ws}$	79.01	99.99	65.40	100.00	90.86	97.09	99.83	99.37
	rate (%)	σ_{ws}	7.86	0.07	10.49	0.03	5.17	3.30	0.35	1.03
	Energy demand	$\bar{x}_{ec}$	7	3	3	19	82	25	185	198
	(Million kw*h)	σ_{ec}	2	0	1	2	12	2	25	28
	Food production	$\bar{x}_{fp}$	6	28	34	79	363	262	695	317
	(Thousand ton)	σ_{fp}	1	2	5	5	38	22	48	23
IV	Water demand	$\bar{x}_{wd}$	298	201	183	226	404	345	1001	1337
	(Million m^3)	σ_{wd}	11	2	9	11	55	16	112	124
	Water supply	$\bar{x}_{ws}$	73.51	99.73	65.99	99.98	87.46	95.05	99.80	99.36
	rate (%)	σ_{ws}	9.01	0.67	10.49	0.05	7.16	4.70	0.36	1.04
	Energy demand	$\bar{x}_{ec}$	5	3	3	16	63	21	151	161
	(Million kw*h)	σ_{ec}	1	0	1	3	13	3	31	34
	Food production	$\bar{x}_{fp}$	6	28	35	79	351	255	692	315
	(Thousand ton)	σ_{fp}	1	2	5	6	44	25	52	24
V	Water demand	$\bar{x}_{wd}$	303	201	185	233	441	352	1077	1421
	(Million m^3)	σ_{wd}	10	2	8	10	50	16	102	115
	Water supply	$\bar{x}_{ws}$	78.17	99.98	65.67	99.99	88.96	96.19	99.82	99.37
	rate (%)	σ_{ws}	7.87	0.14	10.49	0.03	6.15	3.89	0.34	1.03
	Energy demand	$\bar{x}_{ec}$	7	3	3	18	74	23	172	183
	(Million kw*h)	σ_{ec}	2	0	1	3	12	2	28	30
	Food production	$\bar{x}_{fp}$	6	28	34	79	355	258	692	316
	(Thousand ton)	σ_{fp}	1	2	5	5	40	23	48	23
VI	Water demand	$\bar{x}_{wd}$	307	202	187	239	468	357	1132	1484
	(Million m^3)	σ_{wd}	11	2	9	10	48	17	97	114
	Water supply	$\bar{x}_{ws}$	78.80	99.97	65.36	99.99	91.67	97.26	99.82	99.37
	rate (%)	σ_{ws}	8.07	0.15	10.50	0.04	5.05	3.35	0.36	1.04
	Energy demand	$\bar{x}_{ec}$	7	3	3	19	83	25	186	199
	(Million kw*h)	σ_{ec}	2	0	1	3	12	2	26	29
	Food production	$\bar{x}_{fp}$	6	28	34	79	368	264	696	317
	(Thousand ton)	σ_{fp}	1	2	5	6	38	23	51	25
VII	Water demand	$\bar{x}_{wd}$	306	202	187	237	462	356	1119	1470
	(Million m^3)	σ_{wd}	11	2	9	11	51	18	103	119
	Water supply	$\bar{x}_{ws}$	78.65	99.95	65.40	99.99	91.29	96.95	99.82	99.36
	rate (%)	σ_{ws}	8.19	0.22	10.51	0.05	5.53	3.64	0.37	1.06
	Energy demand	$\bar{x}_{ec}$	7	3	3	19	81	24	183	195
	(Million kw*h)	σ_{ec}	2	0	1	3	13	2	28	31
	Food production	$\bar{x}_{fp}$	6	28	34	79	367	263	696	317
	(Thousand ton)	σ_{fp}	1	2	5	6	40	24	53	25

water storage capacity for regulating the local water availability by the reservoir operation. The impacts of water availability uncertainty on the water supply slightly increased, and the standard deviation of the water supply rate increased from 9.20% to 10.49%. The uncertainty of the water released from Z13 increased, with the coefficients of variation increasing from 0.12 under scenario II to 0.13 under scenario III. The water released from Z13 then flowed into the downstream Z14 through the river network. Interestingly, the water supply in Z14 was ensured, and the uncertainty of water flow from Z13 had little impacts on its water supply. As the main water availability source in Z14 was from the main stream of Hanjiang River, there was a large water storage capacity from the R3 Danjiangkou reservoir (with a total storage of 33.91 billion m^3), as shown in Fig. 3, to regulate the water availability uncertainty and ensure water supply. The impacts of the water availability uncertainty in upstream Z13 on the water supply in downstream Z14 decreased. The water supply rates in Z14 under scenarios II, and III were greater than 91.62%, and their standard deviations were less than 0.64%. The water supply rates in Z13 were less than 65.40%, and the corresponding standard deviations were greater than 10.49%. Thus, water availability uncertainty was alleviated through the routes (iv) from Z13 to Z14. A similar uncertainty propagation can be found in routes (i) from Z25 to Z26, and route (ii) from Z2 to Z3. Most of the water availability in Z25 and Z26 was from the main stream of the Hanjiang River that was regulated by the Dangjiangkou reservoir. Their water supplies were ensured, and the impacts of uncertainty of local water availability were decreased by the upstream reservoir operation. If the water resources allocation model was considered, the water supply rates in Z25 and Z26 were more than 99% with small standard deviations. As

Table 7
The amount of water flowed from the upstream to downstream operational zones (million m^3).

Scenario	Variable	**Z25 to Z26** by route (i)	**Z2 to Z3** by route (ii)	**Z19 to Z21** by route (iii)	**Z13 to Z14** by route (iv)
I	$\overline{x}_{rw}$	905	187	310	79
	σ_{rw}	10	1	3	1
	Cv_{rw}	0.01	0.00	0.01	0.01
II	$\overline{x}_{rw}$	469	141	126	66
	σ_{rw}	41	15	24	8
	Cv_{rw}	0.09	0.10	0.19	0.12
III	$\overline{x}_{rw}$	827	183	279	77
	σ_{rw}	68	14	32	10
	Cv_{rw}	0.08	0.08	0.11	0.13
IV	$\overline{x}_{rw}$	736	167	228	75
	σ_{rw}	81	17	34	10
	Cv_{rw}	0.11	0.10	0.15	0.13
V	$\overline{x}_{rw}$	791	180	256	76
	σ_{rw}	73	14	33	10
	Cv_{rw}	0.09	0.08	0.13	0.13
VI	$\overline{x}_{rw}$	830	182	282	77
	σ_{rw}	70	15	34	10
	Cv_{rw}	0.08	0.08	0.12	0.13
VII	$\overline{x}_{rw}$	820	182	277	76
	σ_{rw}	74	15	36	10
	Cv_{rw}	0.09	0.08	0.13	0.13

the water flowed along with the route (ii) from Z2 to Z3 with high uncertainty and the standard deviations were 15 and 14 million m^3, and the coefficients of variation of 0.10 and 0.08 under scenario II and scenario III, respectively. Water availability in Z3 was regulated by the R1 Sanliping and R2 Siping reservoirs, respectively as shown in Fig. 3. The water supply rate in Z3 was 99.99%, and its standard deviation was 0.07% under the scenario III, whereas the water supply rate was 79.01%, and its standard deviation was 7.86% in Z2. The impacts of the upstream water availability uncertainty on water supply were alleviated. As the water storage capacities in both Z19 and Z21 were insufficient to cover the corresponding water demands, and they were connected through the route (iii), the upstream water availability uncertainty did not fade as the standard deviations of the water supply rate were 4.68% and 4.63% in Z19 and Z21, respectively. To quantify the upstream water availability uncertainty propagation to downstream, the joint distributions of both the water availability and water shortage rate in Z19, water availability in Z19 and the water shortage rate in Z21 under scenarios II, and III were estimated. Their conditional distributions were determined based on the joint distributions as shown in Figs. 8, and 9, respectively.

As there was no water resources allocation model in the scenario II, the water shortage rates in Z19 fell between 8% and 45%. There were little differences between the cumulative density function curves shown in Fig. 8(a), if the water availability was less than 800 million m^3. The water shortage rate was typically greater than 15%, which was the critical value of evoking the water shortage awareness accumulation under scenario II, leading to an increase in environmental awareness. The evolution of environmental awareness was accompanied by uncertainty due to the noises as discussed in Section 4.2.1. If the environmental awareness value exceeded its critical value, environmental awareness feedback impacted the evolution of water demand by regulating socioeconomic expansion. The uncertainty then propagated into the water demand and further into the water supply and water shortage rate. Therefore, the water shortage rate uncertainty was considerable because of the model stochasticity when water availability was low, and further challenged the whole WEFS through its nexus. Since the water availability was greater than 800 million m^3, the water shortage decreased remarkably. The water shortage rates were often less than its critical value as shown in Fig. 8(a). Environmental awareness decreased, and the impacts of environmental awareness feedback on socioeconomic variables also diminished. The uncertainty of water demand decreased, and the uncertainty of the water shortage rate decreased. The water shortage rates interval for the most distribution gradually narrowed from 8%–45% to 8%–12% as the water availability increased from 800 to 1400 million m^3 shown in Fig. 8(a). The uncertainty of the co-evolution of the WEFS decreased through its nexus. If the water availability was greater than 1400 million m^3, the corresponding water shortage rates were less than the critical value. Little environmental awareness accumulated, and environmental awareness feedback was rarely triggered. The uncertainty of the WEFS nexus was mainly due to the noises in the dynamics of socioeconomic variables, and its impacts on the WEFS nexus were much smaller than those from the water availability uncertainty as discussed in Section 4.1. As the water released from Z19 flowed into Z21 through the route (iii), the water availability uncertainty in Z19 propagated into Z21 from upstream to downstream. The average value and standard deviation of the water flowing from Z19 to Z21 were 126 and 24 million m^3, respectively with the coefficient of variation of 0.19. The uncertainty of the water supply in Z21 increased owing to the uncertainty propagation of the water availability in Z19. If the water availability was less than 800 million m^3, the water shortage rate in Z21 fell between 8% and 25% as shown in Fig. 8(b). The water supply uncertainty in Z21 was remarkably increased by the uncertainty propagation of water availability in upstream Z19, which was the response of the water supply in Z21 to the water

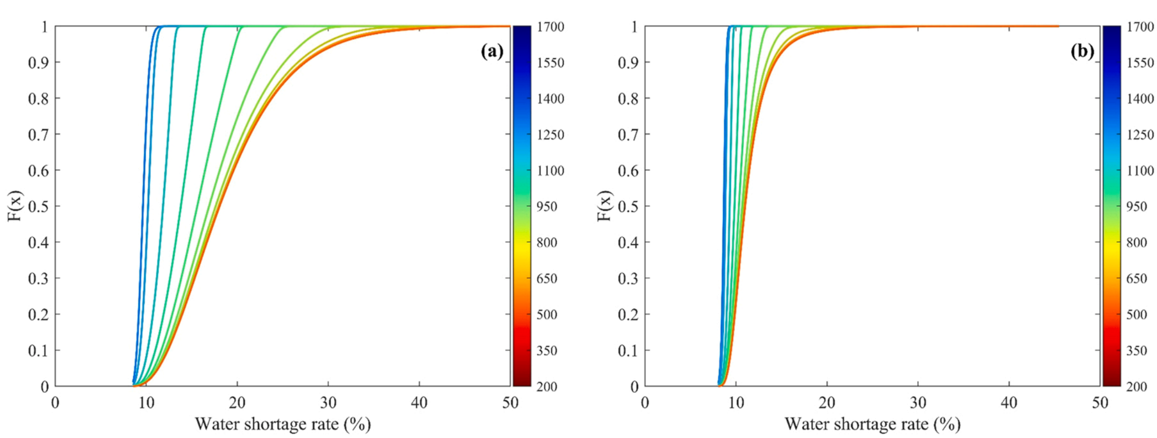

Fig. 8. The conditional distributions of the water availability and water shortage rate in Z19 and Z21 under scenario II: (a) the cumulative density functions (derive from Frank copula) of the water shortage rate under varied water availability (million m^3) in Z19; (b) the cumulative density functions (derive from Frank copula) of the water shortage rate in Z21 under varied water availability (million m^3) in Z19. The similar Figs. 9, 10, 11, 12 and 13 were based on the results from the scenarios III, IV, V, VI and VII, respectively.

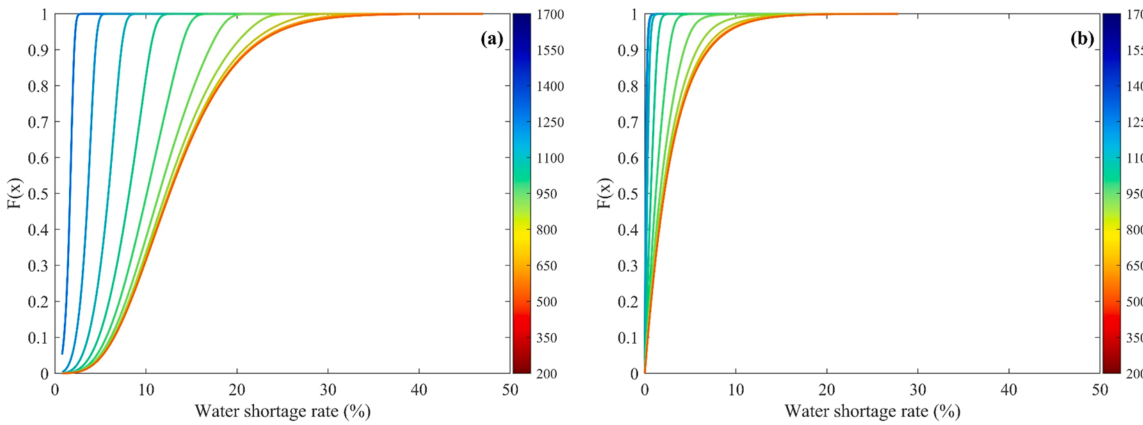

Fig. 9. The conditional distributions of water availability and water shortage rate in Z19, and Z21 under the scenario III (the cumulative density functions in (a) and (b) were derived from Gaussian and Frank copulas, respectively).

availability uncertainty in Z19.

As the water resources allocation model was taken under scenario III, the water shortage in Z19 decreased through reservoir operation, benefiting the co-evolution of the WEFS nexus. The average values of water demand, energy demand, and food production remarkably increased from 248 million m^3 to 466 million m^3, 26 million kw*h to 82 million kw*h, and 332 thousand tons to 363 thousand tons, respectively. The average water supply rate increased from 84.42% to 90.86%, and the corresponding water demand significantly increased. The critical water availability to ensure the water supply in Z19 decreased from 1400 million m^3 under scenario II to 1250 million m^3 under scenario III, as the local water availability was effectively regulated through water resources allocation. The water shortage rate was less than 7% and did not exceed its critical value shown in Fig. 9(a), which was much smaller than the corresponding water shortage rate of 15% shown in Fig. 8(a). Thus, there was a low-level of environmental awareness. The co-evolution of the WEFS nexus was slightly affected by environmental awareness feedback on socioeconomic expansion. The uncertainty in water shortage rate increased with a decrease in water availability when the water availability ranged from 1250 to 800 million m^3. The interval of the water shortage rate expanded from 0–7% to 0–30% shown in Fig. 9(a), whereas the corresponding interval expanded from 8%–12% to 8%–45% shown in Fig. 8(a). As the decreasing water demand was often less than the decreasing water availability, the water shortage rate might have exceeded its critical value in evoking the accumulation of environmental awareness. Thus, water demand uncertainty increased with increasing environmental awareness and further propagated into the WEFS through its nexus. If the water availability was less than 800 million m^3, the water shortage was considerable and cannot be completely relieved by water resources allocation. The water shortage rate fell between 0 and 30% shown in Fig. 9(a) and easily exceeded the critical value. There was high-level environmental awareness, which further altered the evolution of socioeconomic variables for water demand projection through its feedback under the impacts of noises. Owing to the water demand uncertainty, the water supply uncertainty increased, and the uncertainty of the WEFS further increased through its nexus. As the water supply in Z19 was ensured by water resources allocation, the average value of the water flowing from Z19 to Z21 increased from 126 to 279 million m^3, and the coefficient of variation decreased from 0.19 to 0.11. The water supply in Z21 was regulated by the R17 Gaoguan reservoir shown in Fig. 3, and the impacts of the water availability uncertainty in Z19 on the water supply in Z21 were alleviated. The average water supply rate increased from 86.06% to 97.09%. The water shortage rate in Z21 mainly fell in the range of 0–7% with varied water availability as shown in Fig. 9(b). All water shortage rates were below the critical value, and the environmental awareness accumulation was rarely evoked. The impacts of the water availability uncertainty of upstream Z19 on downstream Z21 were effectively alleviated through the regulations on water flow by the R16 Huiting reservoir in Z19 and R17 Gaoguan reservoir in Z21. The standard deviation of water supply rate in Z21 decreased from 4.48% to 3.3%. The water supply uncertainty had little impacts on the evolution of energy demand, and food production. And their standard deviations decreased from 2.2 to 2.1 million kw*h, and from 27 to 22 thousand tons, respectively.

Therefore, the water storage capacity is vital in alleviating the uncertainty propagation in the WEFS nexus. The larger the water storage capacity size, the greater the alleviation of the water availability uncertainty on water supply through reservoir operation. As environmental awareness decreases, the uncertainty from environmental awareness feedback decreases during its propagation in the WEFS nexus. The smaller the water storage capacity size, the fewer the alleviation of water availability uncertainty on water supply. The water availability uncertainty propagated into the water supply, and the water supply uncertainty increased, particularly when the water availability could not satisfy water demand. Thus, environmental awareness increased. Environmental awareness feedback under the impacts of noises can lead to the uncertainty of socioeconomic expansion. The uncertainty further propagated into the water demand, and increased the uncertainty of the co-evolution of the WEFS of downstream zones through the water flowing from upstream into downstream zones.

The proposed framework for assessing the effects of water resources allocation on the uncertainty propagation in the WEFS nexus can aid the comprehensive resources management of water, energy and food in areas where the WEFS is remarkably altered by upstream water availability uncertainty, especially for the transboundary river basins. As the riparian countries have different developmental goals, the different water resources management strategies from upstream to downstream have become an important issue. For instance, the Mekong River basin in Asia (Gao et al., 2021), Nile River basin in Africa (Elsayed et al., 2020), and Columbia River basin in North America (Zhang et al., 2021a). Taking the Nile River basin as a case, the WEFS safety of downstream Egypt can be severely challenged by the water availability uncertainty of upstream Sudan. With the reservoir operation of the upstream Aswan Dam, the upstream water availability uncertainty was effectively decreased and the water supply was significantly increased, which further ensured the rapid socioeconomic expansion of Egypt through its nexus (Strzepek et al., 2008). The proposed framework has considerable potential for riparian countries' cooperation in transboundary river basins to handle the uncertainty propagation in the WEFS nexus.

4.3.2. Impacts of water resources allocation schemes on the uncertainty propagation in the WEFS nexus

The uncertainty propagation showed little response to the different water resources allocation schemes under scenarios III, IV, V, VI, and VII through the routes (i), (ii), and (iv). The varied $Q_{release}$ values determined the amount of water release from the reservoir, and influenced the water supply uncertainty as discussed in Section 4.2.2. The average values of water flow from upstream to downstream from Z25 to Z26 through the route (i), from Z2 to Z3 through route (ii), and from Z13 to Z14 through route (iv) ranged from 736 to 827 million m^3, from 167 to 183 million m^3, from 75 to 77 million m^3, respectively. In comparison, the corresponding standard deviations ranged from 14 to 17 million m^3, from 68 to 81 million m^3, from 9.9 to 10.2 million m^3, respectively. The water availability uncertainties propagated downstream, but were efficiently alleviated through the reservoir operation with large water storage capacities in downstream zones as discussed in Section 4.3.1. Thus, water supplies were ensured and there were few differences in the water supply rates in Z26, Z3, and Z14 under different water resources allocation schemes. As the water storage capacities of downstream zones through the route (iii) were insufficient to satisfy the water demands, the water shortages in downstream zones were related to the $Q_{release}$ values. The uncertainty propagation of water availability was sensitive to water resources allocation schemes through reservoir operation. The conditional distributions of water availability and water shortage rate in Z19 and Z21 reflected the impacts of water resources allocation schemes on the uncertainty propagation through the route (iii) as shown in Figs. 10, 11, 12, and 13 under scenarios IV, V, VI, and VII, respectively.

The $Q_{release}$ value decreased from 1.00 under scenario III to 0.75, and 0.50 under scenarios V and IV, respectively. The uncertainty in the water shortage rates in both Z19 and Z21 increased. A smaller $Q_{release}$ value indicated the decreased water release from the reservoir. The average water supply rate in Z19 decreased from 90.86% under scenario III to 88.96% and 87.46% under scenarios V and IV, respectively. The corresponding standard deviations increased from 5.17% to 6.15% and 7.16%, respectively. A lager environmental awareness has been accumulated. Subsequently, the impacts of environmental awareness feedback on socioeconomic expansion for water demand projection increased. The uncertainty of water demand propagated into the water supply through the water resources allocation. The average water flow from Z19 to Z21 decreased from 279 million m^3 under scenario III to 256 and 228 million m^3 under scenarios V and IV, respectively, while their standard deviation increased from 32 to 33 and 34 million m^3, respectively. Thus, the water supply uncertainty in Z21 increased owing to the increasing uncertainty of the water flow from Z19. As the storage capacity of the R17 Gaoguan reservoir was insufficient to alleviate the water availability uncertainty propagated from Z19, the WEFS uncertainty in Z21 increased through its nexus as discussed in Section 4.3.1.

The standard deviations of water demand, energy demand, and food production in Z21 increased from 46 million m^3, 12 million kw*h, and 38 thousand tons under scenario III, to 50 million m^3, 12 million kw*h, and 40 thousand tons under scenario V and 55 million m^3, 13 million kw*h, and 44 thousand tons under scenario IV, respectively. Interestingly, the smaller the $Q_{release}$ value, the larger the uncertainty of water shortage rates, particularly when the water availability was limited as shown in Figs. 9, 10 and 11. If the water availability in Z19 was less than 800 million m^3, the interval of water shortage rate in Z19 expanded from 0% to 33% under scenario III to 0–38% and 0–42% under scenarios V and IV, respectively. As the water supply decreased with decreasing $Q_{release}$ value, the water shortage increased, and further increased the environmental awareness. The uncertainty of environmental awareness due to its noises propagated into water demand through environmental awareness feedback on socioeconomic sectors. Water demand uncertainty further increased the uncertainties of the water supply and water shortage rate through water resources allocation. There were few differences between the cumulative density function curves of the water shortage rates in Z19 and Z21 as shown in Figs. 9, 10 and 11 when the water availability in Z19 was more than 1400 million m^3, as their water supplies were ensured.

A similar method can be used to analyze the schemes with larger $Q_{release}$ values under scenarios VI and VII (e.g., the $Q_{release}$ value were 1.25 and 1.50, respectively). Although water release increased with a larger $Q_{release}$ value, the water supply in Z19 barely increased. The average water supply rate ranged from 90.86% to 91.67%, and the standard deviation ranged from 5.05% to 5.17%. It was more difficult to maintain the reservoir at its normal water level with a larger $Q_{release}$ value. Although the water supply can be ensured in the flood season, the water supply stress during the dry season increased with limited water storage capacity and water availability. Thus, there were few differences between the cumulative density function curves of the water shortage rates in Z19 and Z21 as shown in Figs. 9, 12 and 13. It was found that the uncertainty propagation of water availability was insensitive to the water resources allocation schemes. Therefore, policymakers have two manners to handle the uncertainty propagation in the WEFS nexus: (a) implementing optimal water resources allocation schemes in the area with few regulating capacity of the water system within a basin; and (b) regulating the local socioeconomic expansion to keep the water demand from over-speed increase. As local water safety is ensured, the water availability uncertainty propagated from upstream can be effectively alleviated, and further the WEFS can be ensured through its nexus.

5. Conclusion

This study proposed a framework to assess the effects of water resources allocation on the uncertainty propagation in the WEFS nexus for

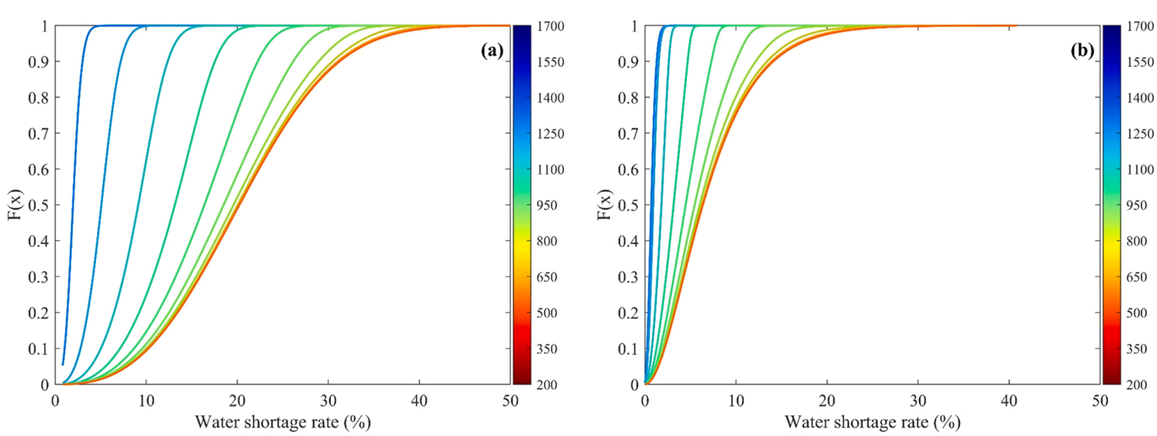

Fig. 10. The conditional distributions of water availability and water shortage rate in Z19, and Z21 under scenario IV (the cumulative density functions in (a) and (b) were derived from Gaussian and Frank copulas, respectively).

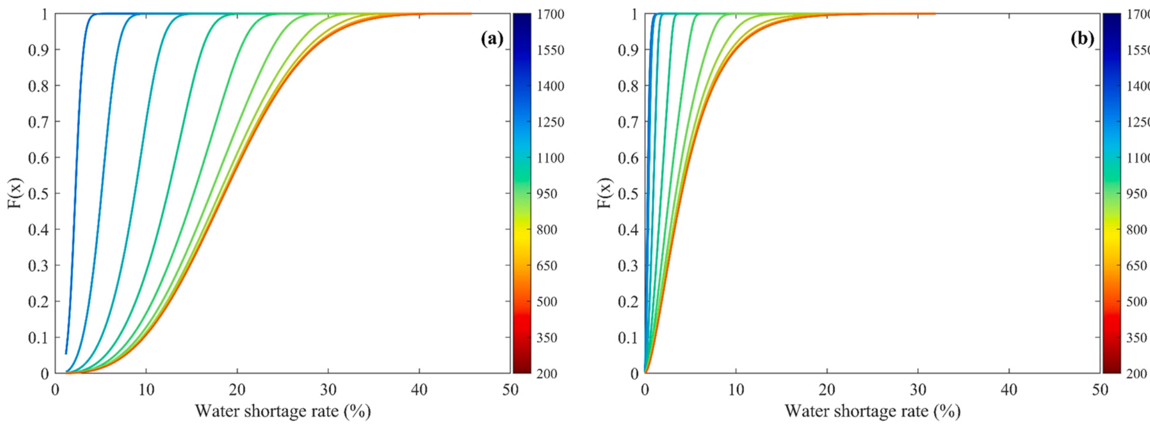

Fig. 11. The conditional distributions of water availability and water shortage rate in Z19, and Z21 under scenario V (the cumulative density functions in (a) and (b) were derived from Gaussian and Frank copulas, respectively).

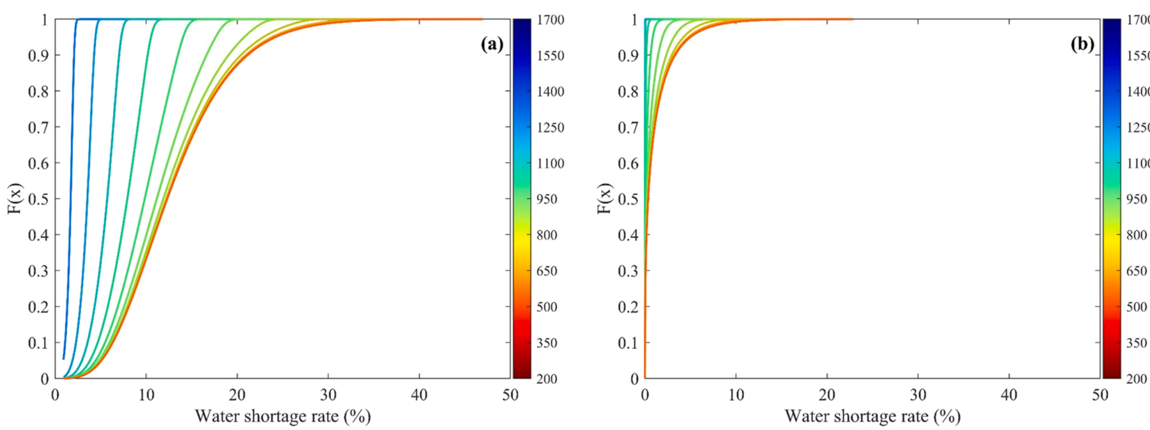

Fig. 12. The conditional distributions of water availability and water shortage rate in Z19, and Z21 under scenario VI (the cumulative density functions in (a) and (b) were derived from Gaussian and t copulas, respectively).

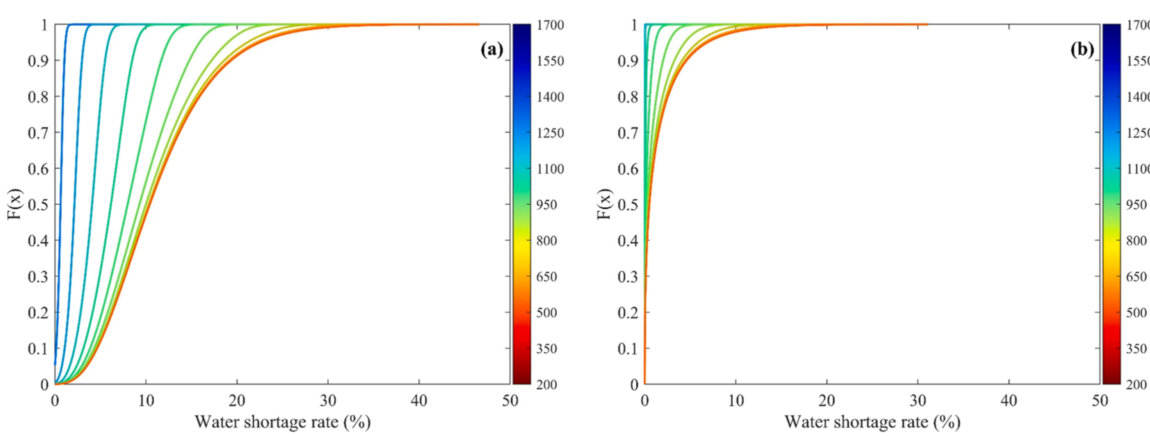

Fig. 13. The conditional distributions of water availability and water shortage rate in Z19, and Z21 under scenario VII (the cumulative density functions in (a) and (b) were derived from Gaussian and t copulas, respectively).

the comprehensive management of water, energy and food under uncertainties. The white Gaussian noises were integrated into seven primary governing equations of the system dynamic model for the WEFS nexus to express the uncertainty of the model structure, transforming the WEFS nexus model from deterministic to stochastic. The copula function was adopted to quantify the uncertainty propagation by estimating the joint distributions between the water availability and shortage rate in the upstream and downstream zones based on the Monte Carlo simulation of the stochastic WEFS nexus model. The effects of water resources allocation on the uncertainty propagation in the WEFS nexus were analyzed by investigating the response of WEFS to different water resources allocation schemes.

According to the results of the case study in the MLHRB, China, water availability uncertainty is the main source of the uncertainty in the WEFS nexus. A rational water resources allocation scheme can efficiently improve water shortage, and diminish the impacts of water availability uncertainty on water supply through reservoir operation. Food production increases remarkably as the agricultural water supply is ensured. High-level environmental awareness evoked by water or food shortages decreases, and ensures the co-evolution of the WEFS nexus. The water availability uncertainty in the upstream zone propagates to downstream zone by the water flow through their hydrologic connections. The water storage capacity of a reservoir for water regulation in an operational zone is the vital factor in regulating the uncertainty propagation within a basin. If there is sufficient water storage capacity in a zone, the impacts of water availability uncertainty in the upstream zone can be alleviated through reservoir operation. There is no significant response of the WEFS through its nexus to different water resources allocation schemes. If there is few water storage capacity in a zone, its water supply is significantly influenced by water availability uncertainty in the upstream zone. Water supply is hardly ensured, and is sensitive to different water resources allocation schemes. Water and food shortages evoke an accumulation of environmental awareness. Environmental awareness feedback under the impacts of model structure uncertainty (i.e., the noises) further increases the water demand uncertainty by altering socioeconomic expansion, particularly when the water availability is much less than the water demand. Then, the water supply uncertainty increases, and propagates into the WEFS through its nexus.

Water availability uncertainty is the primary uncertainty for the co-evolution of the WEFS nexus. In this study, the PDF of water availability was estimated by stationary hydrologic frequency analysis method. However, the stationary assumption of water availability has been remarkably challenged under the impacts of human activities and climate change. The nonstationarity of water availability can bring risks to the WEFS through its nexus, and further challenge sustainable development goals. Therefore, more attention should be paid to the uncertainty analysis of the WEFS nexus under nonstationary water availability conditions.

Declaration of Competing Interest

The authors declare that they have no known competing financial interests or personal relationships that could have appeared to influence the work reported in this paper.

Data availability

Data will be made available on request.

Acknowledgements

The authors gratefully acknowledge the financial support from National Key Research and Development Project of China (2022YFC3202803) and the National Natural Science Foundation of China (Nos. 51879194, 91647106 and 51579183).

Declaration of Competing Interest

The authors declare that they have no conflict of interest.

Appendix A. Supporting information

Supplementary data associated with this article can be found in the online version at doi:10.1016/j.agwat.2023.108279.

References

An, R.H., Liu, P., Feng, M.Y., Cheng, L., Yao, M.L., Wang, Y.B., Li, X., 2021. Resilience analysis of the nexus across water supply, power generation and environmental systems from a stochastic perspective. J. Environ. Manag. 289, 112513 https://doi.org/10.1016/j.jenvman.2021.112513.

Bilgen, S., 2014. Structure and environmental impact of global energy consumption. Renew. Sustain. Energy Rev. 38, 890–902. https://doi.org/10.1016/j.rser.2014.07.004.

Cai, X.M., Wallington, K., Shafiee-Jood, M., Marston, L., 2018. Understanding and managing the food-energy-water nexus - opportunities for water resources research. Adv. Water Resour. 111, 259–273. https://doi.org/10.1016/j.advwatres.2017.11.014.

Castelletti, A., Galelli, S., Restelli, M., Soncini-Sessa, R., 2010. Tree-based reinforcement learning for optimal water reservoir operation. Water Resour. Res. 46, W09507 https://doi.org/10.1029/2009WR008898.

Changjiang Water Resources Commission (CWRC), 2016, Integrated Water Resources Planning of Hanjiang River Basin, Wuhan, China. (in Chinese).

Chen, L., Singh, V.P., Guo, S.L., Mishra, A.K., Guo, J., 2013. Drought analysis using Copulas. J. Hydrol. Eng. 18, 797–808. https://doi.org/10.1061/(ASCE)HE.1943-5584.0000697.

Chen, L., Singh, V.P., Lu, W.W., Zhang, J.H., Zhou, J.Z., Guo, S.L., 2016. Streamflow forecast uncertainty evolution and its effect on real-time reservoir operation. J. Hydrol. 540, 712–726. https://doi.org/10.1016/j.jhydrol.2016.06.015.

Chen, Y.Z., Li, J., Lu, H.W., Yan, P.D., 2021. Coupling system dynamics analysis and risk aversion programming for optimizing the mixed noise-driven shale gas-water supply chains. J. Clean. Prod. 278, 123209 https://doi.org/10.1016/j.jclepro.2020.123209.

Di Baldassarre, G., Sivapalan, M., Rusca, M., Cudennec, C., Garcia, M., Kreibich, H., Konar, M., Mondino, E., Mard, J., Pande, S., Sanderson, M.R., Tian, F.Q., Viglione, A., Wei, J., Wei, Y.P., Yu, D.J., Srinivasan, V., Bloschl, G., 2019. Sociohydrology: scientific challenges in addressing the sustainable development goals. Water Resour. Res. 55, 6327–6355. https://doi.org/10.1029/2018WR023901.

D'Odorico, P., Davis, K.F., Rosa, L., Carr, J.A., Chiarelli, D., Dell'Angelo, J., Gephart, J., MacDonald, G.K., Seekell, D.A., Suweis, S., Rulli, M.C., 2018. The global food-energy-water nexus. Rev. Geophys. 56, 456–531. https://doi.org/10.1029/2017RG000591.

Elsayed, H., Djordjevic, S., Savic, D.A., Tsoukalas, I., Makropoulos, C., 2020. The Nile Water-Food-Energy Nexus under Uncertainty: Impacts of the Grand Ethiopian Renaissance Dam. J. Water Resour. Plan. Manag. 146. https://doi.org/10.1061/(ASCE)WR.1943-5452.0001285.

Feng, M.Y., Liu, P., Li, Z.J., Zhang, J.W., Liu, D.D., Xiong, L.H., 2016. Modeling the nexus across water supply, power generation and environment systems using the system dynamics approach: Hehuang Region, China. J. Hydrol. 543, 344–359. https://doi.org/10.1016/j.jhydrol.2016.10.011.

Feng, M.Y., Liu, P., Cai, X.M., Wallington, K., Shi, L.S., Li, Y., 2019. Understanding the Resilience of Soil Moisture Regimes. Water Resour. Res. 55, 7541–7563. https://doi.org/10.1029/2018WR024495.

Fuchs, S., Karagiorgos, K., Kitikidou, K., Maris, F., Paparrizos, S., Thaler, T., 2017. Flood risk perception and adaptation capacity: a contribution to the socio-hydrology debate. Hydrol. Earth Syst. Sci. 21, 3183–3198. https://doi.org/10.5194/hess-21-3183-2017.

Gao, J.Y., Zhao, J.S., Wang, H., 2021. Dam-Impacted Water-Energy-Food Nexus in Lancang-Mekong River Basin. J. Water Resour. Plan. Manag. 147. https://doi.org/10.1061/(ASCE)WR.1943-5452.0001347.

Govindan, R., Al-Ansari, T., 2019. Computational decision framework for enhancing resilience of the energy, water and food nexus in risky environments. Renew. Sustain. Energy Rev. 112, 653–668. https://doi.org/10.1016/j.rser.2019.06.015.

Guerra, J., Berchin, I.I., Garcia, J., Neiva, S.D., Jonck, A.V., Faraco, R.A., de Amorim, W. S., Ribeiro, J.M.P., 2021. A literature-based study on the water-energy-food nexus for sustainable development. Stoch. Environ. Res. Risk Assess. 35 (95–116), 6. https://doi.org/10.1007/s00477-020-01772-.

Guttal, V., Jayaprakash, C., 2007. Impact of noise on bistable ecological systems. Ecol. Model. 201, 420–428. https://doi.org/10.1016/j.ecolmodel.2006.10.005.

He, S., Guo, S., Yin, J., Liao, Z., Li, H., Liu, Z., 2022. A novel impoundment framework for a mega reservoir system in the upper Yangtze River basin. Appl. Energy 305, 117792. https://doi.org/10.1016/j.apenergy.2021.117792.

Her, Y., Yoo, S.H., Cho, J., Hwang, S., Jeong, J., Seong, C., 2019. Uncertainty in hydrological analysis of climate change: multi-parameter vs. multi-GCM ensemble predictions. Sci. Rep. 9 (4974), 7. https://doi.org/10.1038/s41598-019-41334-.

Hoff, H., 2011. Understanding the nexus. In: Background Paper for the Bonn 2011 Conference. The Water, Energy and Food Security Nexus. Stockh. Environ. Inst.

Hubei Provincial Department of Water Resources (HPDWR), 2014, Dispatching schedules of Hubei provincial large reservoirs, Wuhan, China. (in Chinese).

Huntington, H.P., Schmidt, J.I., Loring, P.A., Whitney, E., Aggarwal, S., Byrd, A.G., Dev, S., Dotson, A.D., Huang, D., Johnson, B., Karenzi, J., Penn, H.J.F., Salmon, A., Sambor, D.J., Schnabel, W.E., Wies, R.W., Wilber, M., 2021. Applying the food-energy-water nexus concept at the local scale. Nat. Sustain. 4 (672–679), 1. https://doi.org/10.1038/s41893-021-00719-.

Jeremiah, E., Sisson, S., Marshall, L., Mehrotra, R., Sharma, A., 2011. Bayesian calibration and uncertainty analysis of hydrological models: A comparison of adaptive Metropolis and sequential Monte Carlo samplers. Water Resour. Res. 47, W07547 https://doi.org/10.1029/2010WR010217.

Ji, L., Wu, T.H., Xie, Y.L., Huang, G.H., Sun, L.J., 2020. A novel two-stage fuzzy stochastic model for water supply management from a water-energy nexus perspective. J. Clean. Prod. 277, 123386 https://doi.org/10.1016/j.jclepro.2020.123386.

Karmakar, S., Simonovic, S.P., 2009. Bivariate flood frequency analysis. Part 2: a copula-based approach with mixed marginal distributions. J. Flood Risk Manag. 2, 32–44. https://doi.org/10.1111/j.1753-318X.2009.01020.x.

Knighton, J., White, E., Lennon, E., Rajan, R., 2014. Development of probability distributions for urban hydrologic model parameters and a Monte Carlo analysis of

model sensitivity. Hydrol. Process. 28, 5131–5139. https://doi.org/10.1002/hyp.10009.
Li, B., Sivapalan, M., Xu, X., 2019. An urban sociohydrologic model for exploration of Beijing's water sustainability challenges and solution spaces. Water Resour. Res. 55, 5918–5940. https://doi.org/10.1029/2018wr023816.
Liu, D.D., Chen, X.H., Lou, Z.H., 2010. A Model for the Optimal Allocation of Water Resources in a Saltwater Intrusion Area: A Case Study in Pearl River Delta in China. Water Resour. Manag. 24, 63–81. https://doi.org/10.1007/s11269-009-9437-y.
Liu, D.D., Guo, S.L., Shao, Q.X., Liu, P., Xiong, L.H., Wang, L., Hong, X.J., Xu, Y., Wang, Z.L., 2018. Assessing the effects of adaptation measures on optimal water resources allocation under varied water availability conditions. J. Hydrol. 556, 759–774. https://doi.org/10.1016/j.jhydrol.2017.12.002.
Loucks, D.P., 2002. Interactive River-Aquifer Simulation and Stochastic Analyses for Predicting and Evaluating the Ecologic Impacts of Alternative Land and Water Management Policies. Kluwer Academic Publishers,, Dordrecht, The Netherlands.
Ma, Y., Li, Y.P., Huang, G.H., 2020. A bi-level chance-constrained programming method for quantifying the effectiveness of water-trading to water-food-ecology nexus in Amu Darya River basin of Central Asia. Environ. Res. 183, 109229 https://doi.org/10.1016/j.envres.2020.109229.
Meng, Y., Lai, Y.C., Grebogi, C., 2020. Tipping point and noise-induced transients in ecological networks. J. R. Soc. Interface 17, 20200645. https://doi.org/10.1098/rsif.2020.0645.
Moges, E., Demissie, Y., Li, H.Y., 2020. Uncertainty propagation in coupled hydrological models using winding stairs and null-space Monte Carlo methods. J. Hydrol. 589, 125341 https://doi.org/10.1016/j.jhydrol.2020.125341.
Muller Schmied, H., Eisner, S., Franz, D., Wattenbach, M., Portmann, F.T., Florke, M., Doll, P., 2014. Sensitivity of simulated global-scale freshwater fluxes and storages to input data, hydrological model structure, human water use and calibration. Hydrol. Earth Syst. Sci. 18, 3511–3538. https://doi.org/10.5194/hess-18-3511-2014.
Nelsen, R.B., 2006. An Introduction to Copulas. Springer,, New York.
Pedro-Monzonis, M., Solera, A., Ferrer, J., Estrela, T., Paredes-Arquiola, J., 2015. A review of water scarcity and drought indexes in water resources planning and management. J. Hydrol. 527, 482–493. https://doi.org/10.1016/j.jhydrol.2015.05.003.
Renard, B., 2011. A Bayesian hierarchical approach to regional frequency analysis. Water Resour. Res. 47, W11513 https://doi.org/10.1029/2010WR010089.
Schmogrow, R., Nebendahl, B., Winter, M., Josten, A., Hillerkuss, D., Koenig, S., Meyer, J., Dreschmann, M., Huebner, M., Koos, C., Becker, J., Freude, W., Leuthold, J., 2012. Error Vector Magnitude as a Performance Measure for Advanced Modulation Formats. Ieee Photonics Technol. Lett. 24, 61–63. https://doi.org/10.1109/LPT.2011.2172405.
Serinaldi, F., 2013. An uncertain journey around the tails of multivariate hydrological distributions. Water Resour. Res. 49, 6527–6547. https://doi.org/10.1002/wrcr.20531.
Shoemaker, L.G., Sullivan, L.L., Donohue, I., Cabral, J.S., Williams, R.J., Mayfield, M.M., Chase, J.M., Chu, C.J., Harpole, W.S., Huth, A., HilleRisLambers, J., James, A.R.M., Kraft, N.J.B., May, F., Muthukrishnan, R., Satterlee, S., Taubert, F., Wang, X.G., Wiegand, T., Yang, Q., Abbott, K.C., 2020. Integrating the underlying structure of stochasticity into community ecology. Ecology 101, e02922. https://doi.org/10.1002/ecy.2922.
Silva, M.A., Amado, C., Loureiro, D., 2018. Propagation of uncertainty in the water balance calculation in urban water supply systems - A new approach based on high-density regions. Measurement 126, 356–368. https://doi.org/10.1016/j.measurement.2018.05.061.
Simonovic, S.P., 2002. World water dynamics: global modeling of water resources. J. Environ. Manag. 66, 249–267. https://doi.org/10.1006/jema.2002.0585.
Sivapalan, M., Savenije, H.H.G., Bloschl, G., 2012. Socio-hydrology: A new science of people and water. Hydrol. Process. 26, 1270–1276. https://doi.org/10.1002/hyp.8426.
Strzepek, K.M., Yohe, G.W., Tol, R.S.J., Rosegrant, M.W., 2008. The value of the high Aswan Dam to the Egyptian economy. Ecol. Econ. 66, 117–126. https://doi.org/10.1016/j.ecolecon.2007.08.019.
Vellend, M., Srivastava, D.S., Anderson, K.M., Brown, C.D., Jankowski, J.E., Kleynhans, E.J., Kraft, N.J.B., Letaw, A.D., Macdonald, A.A.M., Maclean, J.E., Myers-Smith, I.H., Norris, A.R., Xue, X.X., 2014. Assessing the relative importance of neutral stochasticity in ecological communities. Oikos 123, 1420–1430. https://doi.org/10.1111/oik.01493.
Vetter, T., Reinhardt, J., Florke, M., van Griensven, A., Hattermann, F., Huang, S.C., Koch, H., Pechlivanidis, I.G., Plotner, S., Seidou, O., Su, B.D., Vervoort, R.W., Krysanova, V., 2017. Evaluation of sources of uncertainty in projected hydrological changes under climate change in 12 large-scale river basins. Clim. Change 141, 419–433. https://doi.org/10.1007/s10584-016-1794-y.
Vörösmarty, C.J., Green, P., Salisbury, J., Lammers, R.B., 2000. Global water resources: Vulnerability from climate change and population growth. Science 289, 284–288. https://doi.org/10.1126/science.289.5477.284.
West, P.C., Gerber, J.S., Engstrom, P.M., Mueller, N.D., Brauman, K.A., Carlson, K.M., Cassidy, E.S., Johnston, M., MacDonald, G.K., Ray, D.K., Siebert, S., 2014. Leverage points for improving global food security and the environment. Science 345, 325–328. https://doi.org/10.1126/science.1246067.
Wu, Z.H., Liu, D.D., Mei, Y.D., Guo, S.L., Xiong, L.H., Liu, P., Yin, J.B., Zeng, Y.J., 2022. Delayed feedback between adaptive reservoir operation and environmental awareness within water supply-hydropower generation-environment nexus. J. Clean. Prod. 345, 131181 https://doi.org/10.1016/j.jclepro.2022.131181.
Xiao, S.N., Xu, T., Reuschen, S., Nowak, W., Franssen, H.J.H., 2021. Bayesian Inversion of Multi-Gaussian Log-Conductivity Fields With Uncertain Hyperparameters: An Extension of Preconditioned Crank-Nicolson Markov Chain Monte Carlo With Parallel Tempering. Water Resour. Res. 57 e2021WR030313, 10.1029/2021WR030313.
Yin, J.B., Guo, S.L., Liu, Z.J., Yang, G., Zhong, Y.X., Liu, D.D., 2018. Uncertainty Analysis of Bivariate Design Flood Estimation and its Impacts on Reservoir Routing. Water Resour. Manag. 32, 1795–1809. https://doi.org/10.1007/s11269-018-1904-x.
Zeng, X.T., Zhang, J.L., Yu, L., Zhu, J.X., Li, Z., Tang, L., 2019a. A sustainable water-food-energy plan to confront climatic and socioeconomic changes using simulation-optimization approach. Appl. Energy 236, 743–759. https://doi.org/10.1016/j.apenergy.2018.11.086.
Zeng, X.T., Zhang, S.J., Feng, J., Huang, G.H., Li, Y.P., Zhang, P., Chen, J.P., Li, K.L., 2017. A multi-reservoir based water-hydroenergy management model for identifying the risk horizon of regional resources-energy policy under uncertainties. Energy Convers. Manag. 143, 66–84. https://doi.org/10.1016/j.enconman.2017.02.020.
Zeng, X.T., Zhao, J.Y., Wang, D.Q., Kong, X.M., Zhu, Y., Liu, Z.P., Dai, W., Huang, G.H., 2019b. Scenario analysis of a sustainable water-food nexus optimization with consideration of population-economy regulation in Beijing-Tianjin-Hebei region. J. Clean. Prod. 228, 927–940. https://doi.org/10.1016/j.jclepro.2019.04.319.
Zeng, Y.J., Liu, D.D., Guo, S.L., Xiong, L.H., Liu, P., Yin, J.B., Wu, Z.H., 2022. A system dynamic model to quantify the impacts of water resources allocation on water-energy-food-society (WEFS) nexus. Hydrol. Earth Syst. Sci. 26, 3965–3988. https://doi.org/10.5194/hess-26-3965-2022.
Zeng, Y.J., Liu, D.D., Guo, S.L., Xiong, L.H., Liu, P., Yin, J.B., Tian, J., Deng, L.L., Zhang, J.Y., 2021. Impacts of Water Resources Allocation on Water Environmental Capacity under Climate Change. Water 13, 1187. https://doi.org/10.3390/w13091187.
Zhang, J.R., Yang, Y.C.E., Li, H.Y., Shittu, E., 2021a. Examining the food-energy-water-environment nexus in transboundary river basins through a human dimension lens: Columbia River Basin. J. Water Resour. Plan. Manag. 147. https://doi.org/10.1061/(ASCE)WR.1943-5452.0001461.
Zhang, Y.F., Li, Y.P., Huang, G.H., Ma, Y., 2021. A copula-based stochastic fractional programming method for optimizing water-food-energy nexus system under uncertainty in the Aral Sea basin. J. Clean. Prod. 292, 126037 https://doi.org/10.1016/j.jclepro.2021.126037.
Zhang, Y.Y., Shao, Q.X., 2018. Uncertainty and its propagation estimation for an integrated water system model: An experiment from water quantity to quality simulations. J. Hydrol. 565, 623–635. https://doi.org/10.1016/j.jhydrol.2018.08.070.